ELECTRODE LENGTH MEASUREMENT IN ELECTRIC ARC FURNACES

NORMAN BALLARD, B.Sc.(Eng)

26 April 1995

Thesis submitted to the Department of Electrical Engineering of the University of Cape Town in partial fulfilment of the requirements for the Degree of M.Sc.(Eng).

ACKNOWLEDGEMENTS

The author would like to thank the following advisors, colleagues and friends for all their assistance with this project:

Prof M. R. Inggs, UCT
Prof B. Downing, UCT
Mrs C. Pretorius, Mintek
Dr I. Barker, Mintek
Mr G. M. Tattersfield, UCT

SYNOPSIS

Accurate measurement of electrode length in electric arc furnaces will result in decreased maintenance time, and improved plant productivity. This thesis describes the development of a microwave-based Soderberg electrode length-measurement system.

Various methods of electrode-length measurement were investigated, and it was found that a microwave measurement system based on a conventional frequency modulated continuous wave (FMCW) radar presented the most feasible technique. In this system, microwaves are propagated down a waveguide placed in the electrode. As the waveguide melts, they continue propagating in the resulting cavity until they are reflected by the discontinuity at the bottom of the electrode. The time taken for the return journey to the bottom of the electrode and back is measured, and the electrode length calculated.

FMCW radar measures return time by mixing a transmitted linear frequency sweep with the reflection to produce the difference frequency. The resulting beat frequency is then proportional to the distance from the reflecting object. An investigation into the required linearity of the microwave source showed that the linearity is crucial to obtaining high signal-to-noise ratios in the beat frequency and therefore also to achieving good measurement accuracy. Although the designed radar had built-in linearisation capabilities, it was found to be more cost-effective to use a temperature-stabilised linear voltage controlled oscillator.

Ultimately, the accuracy with which electrode length can be determined depends on how accurately the peaks in the beat frequency spectrum can be determined. Various spectral estimation techniques were investigated, and it was found that the fast Fourier transform in conjunction with zero padding and weighted averages provided a good combination of fast, robust and accurate results.

A steel pipe with the same dimensions as the one to be placed in the electrode was used to test the measurement system. Electrode tip erosion was

modelled by moving a reflective plunger up the waveguide. Length measurements were performed between 4.5m and 6.9m at one-centimetre intervals. The RMS error associated with the measurements was found to be 1.37cm, and the linearity of the system was excellent. Further experiments up to 9m long confirmed the accuracy and linearity. Finally, a 40cm-long section of Soderberg electrode was placed at the end of the electrode to confirm that the waves would continue to propagate after the waveguide had melted. The length-measurement system performed as well as in previous experiments, with the electrode section having no adverse effect on the measurements. Various other experiments to determine the effects of waveguide joints, temperature changes and electrode terminations also had favourable results.

A radar-based system was thus designed to measure the length of Soderberg electrodes in electric arc furnaces. The system was then built and tested, and it was found that it provided excellent measurement accuracy under a range of conditions. The system must now be implemented in a real furnace in order to evaluate the effect of the environment further.

Contents

List of Figures

List of Tables

Chapter 1

INTRODUCTION

Submerged electric arc furnaces have been used since the beginning of the century as a means of melting scrap steel and smelting ores into their associated metals and alloys. As the name *submerged electric arc furnace* suggests, graphite electrodes immersed into the burden (mixture of ores, reducing agents and fluxes) [2, page 1] are used to create an electric arc beneath it. Electrical energy supplied to the electrodes is transferred to the burden in a combination of arc and resistive heating. Since these are low voltage mechanisms (100V-400V) [2, page37], the currents delivered have to be large to provide the necessary energy for the melting process. The high currents are fed to the electrodes through fixed bus bars and heavy duty cables from transformers situated close to the furnace. Contact between the conducting cables and the electrode is maintained by means of brass or copper contact shoes which are held against the electrode using hydraulics or spring pressure.

Traditionally, fixed graphite electrodes that required replacing as they became eroded were used. This replacement was found to be prohibitively expensive due to lost production time. The tapped electrode (Figure 1.1) which was later introduced as the first *continuous* electrode did not require replacing, but excessive wear and breakage were common at the joints between alternate sections.

In the early 1920s, C. W. Soderberg [6] invented the *Soderberg electrode* (Figure 1.2), which, like the threaded electrode, is continuous. The *Soderberg electrode* consists of a tubular steel casing made up of one-to-two-metre sections which are filled with blocks of carbon paste. As the electrode is slipped further towards the furnace, the blocks of carbon paste melt, and then bake, to form solid graphite. The steel casing then melts off, leaving a solid graphite electrode. Steel fins are sometimes welded onto the insides of

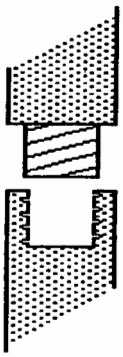

Figure 1.1: Tapped electrodes.

the casings to hold the hardening graphite and to improve the conductivity of the electrode. Feeder pipes used to introduce fines into the furnace may also be inserted.

Knowledge of the length of the electrodes is crucial for many reasons:

1. The furnace operator must not slip the electrode too far, causing it to hit the bottom of the furnace.

2. Maintenance of the reaction zones beneath the electrodes requires accurate knowledge of their length.

3. Power factor correction which reduces electricity costs substantially is simplified if electrode length is known.

Various attempts have been made to estimate electrode length using mathematical models, erosion profiles and measurements of electrical variables affecting the furnace. However, these have produced rough estimates only, and have obtained limited success [2, page 34], [12].

The objective of this study is to investigate various methods of electrode-length determination, and to develop a prototype system which can be used under conditions similar to those encountered in a real furnace. The system should be able to measure the length of the electrode with a resolution greater than 10cm. Although various methods of length determination will be investigated, the main thrust of the project will be towards the use of radar-based techniques.

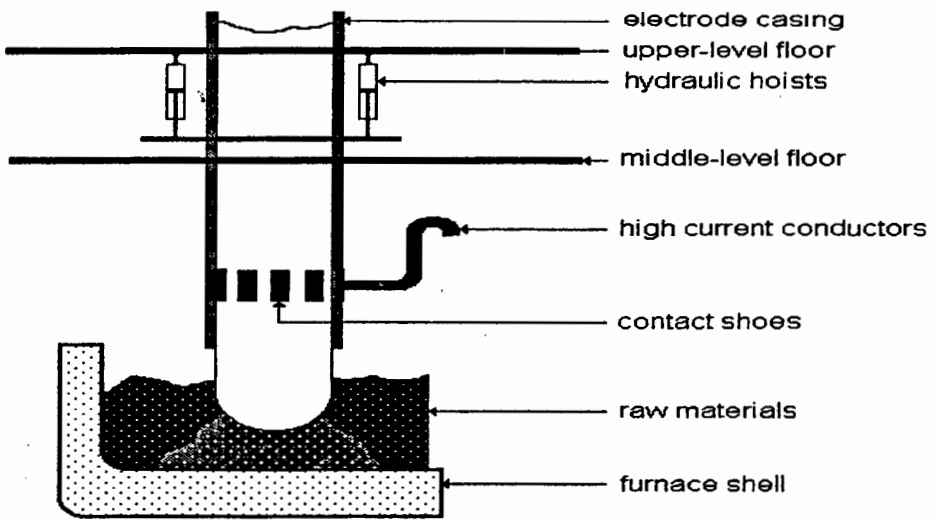

Figure 1.2: Simplified form of a Soderberg electrode.

The requirements of the project are as follows:

1. An investigation into the various electrode-length measurement techniques must be performed, and a suitable technique chosen.
2. A theoretical evaluation of the proposed system must be performed to determine whether it will provide the required resolution.
3. A prototype system must be built and tested to determine its performance.

The length-determination system is to be designed for a *general* electric arc furnace. In other words, it should not matter to the *length-determination system* whether calcium carbide or scrap steel is being melted. Although every effort will be made to consider all aspects of the furnace environment, this will be extremely difficult due to the harsh conditions encountered therein. The prototype developed in this thesis will therefore have to be ruggedised and tested in the real environment.

Various electrode-length-measurement techniques including microwave, ultrasonic and parameter estimation methods are discussed in Chapter Two. Microwave length measurement, in conjunction with a waveguide inserted into the electrode, is found to be the most feasible. The specific microwave measurement technique is then investigated and it is decided that a *frequency modulated continuous wave* (FMCW) radar mounted above the electrode should be used.

Chapter Three deals with the design of the FMCW radar and waveguide to be inserted into the electrode. A trade-off between *phase-locked loop* (PLL) and *conventional* FMCW radar is presented. Conventional FMCW radar is chosen, the system parameters are calculated and the entire system is specified.

The implementation of the hardware is discussed in Chapter Four. The Components that were used, along with the integration process, are described. An evaluation of various signal processing techniques including the fast Fourier transform (FFT), Prony and multiple signal classification (MUSIC) techniques is presented, and it is found that the fast Fourier transform best fits the requirements.

The various experiments performed to evaluate the system are described in Chapter Five. The results show that the system performs well under a variety of conditions, and provides the required resolution.

Chapter 2

REVIEW OF POSSIBLE MEASUREMENT TECHNIQUES

This chapter will review previous attempts to measure electrode length, and will introduce some new concepts. The most promising technique from those presented will be chosen for further research.

The most common electric arc furnace, and therefore the one to be assumed in all discussion, is the circular three-electrode furnace shown in Figure 2.1. In this arrangement, three Soderberg electrodes are held in a ring above the furnace, and extend into the burden. The materials to be melted are carried above the furnace on a conveyor belt, and then gravity-fed into the furnace through chutes. Once melted, the burden produces a slag, which is normally less dense than the melted ore and therefore lies on the surface, and can be removed. The ore is tapped off through tapholes in the sides of the furnace.

2.1 Previous Attempts at Electrode-Length Measurement

The most widely-used technique for electrode-length determination is called sounding. During sounding, the flow of raw materials is stopped, and the burden lowered, so that when the furnace is switched off, and the electrodes raised, one can see their ends, and therefore measure their length. Unfortunately, the technique of sounding can only be used periodically since it results in a significant reduction in the performance of the furnace.

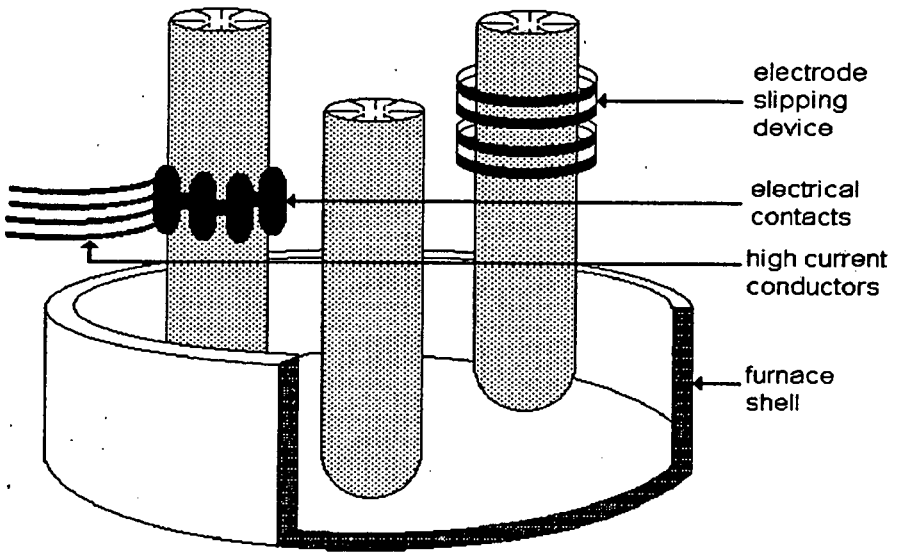

Figure 2.1: Cross section through a three-electrode electric arc furnace.

All the other methods of length determination to be discussed in this chapter are *continuous* methods of electrode determination. By *continuous*, it is meant that the furnace operation should remain unaffected by the length-determination system. The technique of sounding, therefore, does not fall into this category.

2.1.1 Erosion models

The length of an electrode is a function of the rate of slipping and the rate of electrode tip erosion. The rate of electrode slip can be measured with relative ease; however, the rate of tip erosion is an unknown quantity. Physical erosion models that relate erosion rate to power consumed by each electrode have been suggested. The prediction accuracy of the models is dependent on the accuracy with which phase-power measurements can be performed. For still further predictability, the effects of arcing between the electrodes can be taken into consideration.

The erosion models cannot, however, take electrode imperfections, electrode non-homogeneity or tip breaks into account. The errors associated with the electrode erosion models are additive, and should not therefore be relied upon over extended periods of time. For this reason, electrode sounding must still be carried out on a regular basis.

Measurements of electrical arcing, resistance and reactance were used by Barcza [2] to model the length of graphite electrodes. Electrical parameter-

based models have the distinct advantage over erosion models of being able to detect tip breakages. The life of these models can therefore be extended, and the time between soundings increased. The models, however, require certain furnace-specific constants such as the conductivity of the burden, which need to be updated regularly.

2.1.2 Acoustical detection of electrode tips

Under acoustical methods, both audible and ultrasonic frequencies will be included since the mechanisms behind both techniques are similar. Sound waves would be propagated from below the furnace bath, through the furnace shell and burden to be bounced off the electrode tips. Similar techniques have been used by [1] and [8] to measure the thickness of walls and steel plates respectively.

The furnace shell has to be heat resistant, and id designed to have a long life, since renewal is costly both in terms of materials and of loss of production. For this reason, it has a temperature-resistant carbon lining between the burden and the refractory wall. The floor on the inside of the steel furnace shell is covered with up to half a metre of refractory brick, a thin layer of refractory concrete to provide a level surface and then up to seven layers of refractory brick and two layers of carbon blocks [2, page 7,8].

A. Jongens [5] of the acoustical department at the University of Cape Town investigated the possibility of using acoustical measurements to determine the length of electrodes. He found, however, that the complex nature of the furnace shell, and the inconsistent and unpredictable nature of the materials contained within the furnace, would have prevented any accurate measurement from being made in either the audible or ultrasonic frequency range.

2.2 New Electrode-Length-Measurement Ideas Considered

Before a final electrode-length-measurement technique was chosen, many new ideas were considered. Some of the ideas, such as weighing the electrode, could be discounted immediately, whereas others required more thorough investigation. The aim of this chapter is to guide the reader through each technique considered, and to explain the final choice that was made.

2.2.1 Weighing the electrode

The electrode could be suspended in a frame which is mounted on load cells. The load cells would measure the weight of the electrode, from which its length may be calculable. Unfortunately, the weight of the electrode is a complicated function which is affected by the addition of electrode materials, by the buoyancy provided by the slag in the furnace and by erosion of the electrodes. The buoyancy problem could be overcome by lifting the electrode slightly before measurement, but as mentioned before with reference to the technique of sounding, this is undesirable.

Therefore, due to the relative complexity and number of unknown quantities, weight measurement as an indication of electrode length will not be considered any further.

2.2.2 Using the mechanical resonant frequency of the electrode to deduce its length

All physical objects have a natural frequency of vibration, commonly called the resonant frequency. The resonant frequency of a simple pendulum, for instance, is given by:

$$f_{res} = \sqrt{\frac{l}{g}} \tag{2.1}$$

where l is the length of the pendulum and g is the acceleration due to gravity.

This suggests that if the electrode were modelled as a pendulum, and its resonant frequency were measured, then Equation 2.1 could be used to determine its length. An accelerometer placed on the electrode could be used to measure electrode vibration and, therefore, resonant frequency.

Unfortunately the structure holding the electrode and the slag in the furnace would tend to dampen free oscillations, making detection of the resonant frequency difficult. In addition, the resonant frequency may depend on the electrode mass, which, as stated previously, would be extremely difficult to measure.

2.2.3 Inserting an optical fibre into the electrode

If an optical fibre could be inserted into the electrode, laser light could be propagated down the fibre to the bottom of the electrode. The electrode length could then be found using laser interferometry.

The majority of optical fibres melt below 600°C, and would therefore not survive the high temperatures existing in the furnace (2500°C). If an

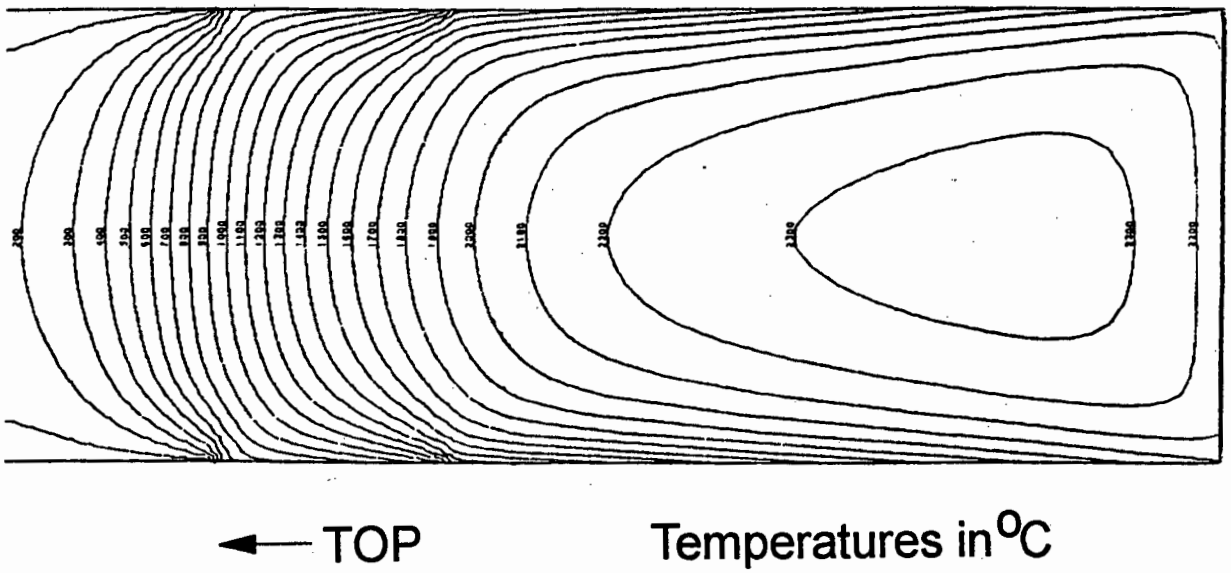

Figure 2.2: Temperature profile of a Soderberg self-baking electrode.

optical fibre were found which could survive the high temperatures in the electrode, then it is improbable that it would melt as it exits the electrode, since, as is shown in Figure 2.2, the hottest point in the furnace is inside the tip of the electrode. Inaccurate results could therefore be obtained.

2.2.4 The insertion of a waveguide into the graphite electrode

A waveguide could be inserted into the graphite electrode. Electromagnetic (EM) energy could then be propagated down the waveguide, reflected at the end and returned. If the time taken for the electromagnetic energy to be transmitted, reflected, and received were determined, then the electrode length could be calculated. Although the strength of the end reflection is unknown, the electrode tip is maintained just above the burden and could therefore be modelled to a first approximation as an open circuit.

The waveguide to be used in the electrode could either be a hollow pipe or a dielectric rod. If a hollow pipe were used, the EM waves would propagate down the tube, bounded by the conductive steel walls. In the dielectric waveguide, they would propagate in the dielectric (a thermally-resistant ceramic rod), being bounded by the graphite of the electrode.

The length of the waveguide, and therefore of the electrode could be measured using any one of the following radar techniques:

- Pulsed radar
- Multi-Frequency Continuous Wave (MFCW) radar

- Stepped frequency radar
- Frequency Modulated Continuous Wave (FMCW) radar

2.2.5 Ground-probing radar techniques

The principle used in ground-probing radar is to transmit electromagnetic energy into the ground with an antenna. Any object or discontinuity in the ground would cause the electromagnetic energy to be reflected. These reflections are received and interpreted to determine the depth of the reflecting source.

The depth to which the ground-probing radar can detect reflecting objects depends on a factor called the *skin depth* of the material being probed. The *skin depth* is the physical depth at which the power density is half (-3dB) of the transmitted power and is given by:

$$\delta_{skin} = \sqrt{\frac{2}{\omega\mu\sigma}} \tag{2.2}$$

where

- δ_{skin} is the skin depth
- ω is the frequency of the electromagnetic energy in $\frac{rad}{s}$
- μ is the magnetic permeability of the material being probed
- σ is the conductivity of the material being probed

Using a frequency of 10GHz, a relative permeability of 1 and a conductivity of 100S/m for graphite, the skin depth has been calculated to be 0.5mm. Therefore, after an electromagnetic wave has propagated 0.5mm into a piece of graphite, its power is halved. From Figure 2.3 (courtesy of Mintek), we see that the conductivity of the graphite electrode increases as its temperature increases, further reducing the skin depth. Therefore, since the ground-probing radar would only be able to detect objects a fraction of a millimetre deep in graphite, it would certainly not be able to detect the end of a 20m electrode.

2.2.6 Sensing the hottest point in the furnace

Since the electrode tip is the hottest point in the furnace, one could use sensors situated around the furnace bath to determine the position of the hottest point within the bath, and therefore of the tip of the electrode.

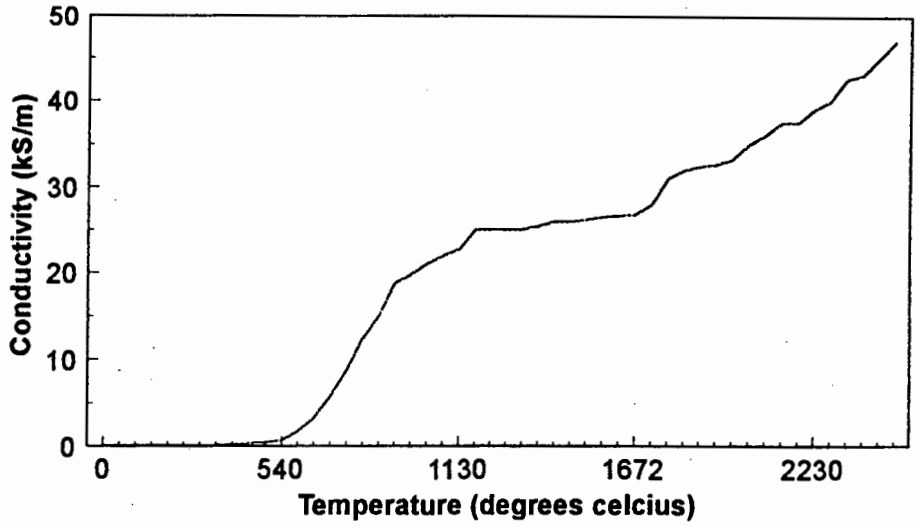

Figure 2.3: Conductivity of graphite as a function of temperature.

Unfortunately, the time it takes for heat energy to reach the sides of the bath is far too long; and, in addition, convection currents in the ore could cause heat pockets to move around, causing spurious results.

2.3 Summary of Electrode-Measurement Techniques

Those measurement techniques which require a regular sounding campaign to be carried out do not fulfil the requirement that the system should be *on-line*. From the other techniques suggested, acoustical methods, mass determination, resonant frequency analysis, optical fibre insertion, heat sensing and ground-probing radar could be discounted quickly.

So in conclusion, the use of a radar technique to measure the length of a waveguide inserted into an electrode has been found to be the most feasible method among a number of possibilities. More specific determinations, of both the type of radar and of the waveguide to be used, will require further investigation.

Chapter 3

CHOICE AND DESIGN OF GUIDING STRUCTURE

Microwaves are to be propagated down a waveguide that has been inserted in the electrode. At some point the waveguide will melt, and the microwaves must continue propagating down the resulting cavity. The various aspects of the guiding structure to be investigated are:

- The type of waveguide to be used
- The frequency of the propagated energy
- The form of electromagnetic energy to be propagated down the electrode
- The size and cross-sectional shape of the waveguide
- Techniques of launching electromagnetic energy into the waveguide
- The signal velocity in the waveguide
- The losses incurred when the electromagnetic energy propagates in the cavity subsequent to the melting of the steel waveguide

3.1 The Type of Waveguide to be Used

Waveguides can be classified into two main types: dielectric waveguides or hollow waveguides. A dielectric waveguide consists of a solid central core surrounded by a material with different dielectric properties. In the case of an electrode, the central core could be a heat-resistant ceramic, and the surrounding material would be the graphite of the electrode. A hollow

waveguide would consist of either round or rectangular conductive tubing. The various merits of the two waveguide types are discussed below:

- Low-cost steel piping of standard dimension could be used to form the hollow waveguide whereas a more costly ceramic rod would be required for the dielectric version.

- Slag or ore from the furnace may cause clogging of the hollow waveguide. It could however be flushed periodically with compressed air. Since the dielectric guide is solid, it would be immune to this problem.

- The joining of hollow waveguide sections could be performed with a weld or simple clamp, whereas the dielectric waveguide would require more precise alignment to prevent significant losses at joints.

- The attenuation suffered in the hollow waveguide would be simple to calculate until the guiding structure melts. Thereafter, the attenuation due to the walls of the cavity in the electrode would be unknown. The attenuation in the dielectric waveguide would depend on the nature of the graphite sheath surrounding the core, and would therefore also be difficult to estimate.

- The dielectric waveguide relies on the graphite of the electrode being able to provide a dielectric coating for the central core. In its first phase, however, the graphite in a Soderberg electrode is in the form of blocks of graphite paste. It is not until the blocks of paste melt that they would be able to act as a continuous coating for the waveguide core. The dielectric waveguide would therefore have to be supplied with its own sheath already in place. This would further complicate the joining of waveguide sections, and would increase the cost of the system

- The ceramic core to be used in a dielectric waveguide would have to be chosen with a melting point and erosion rate similar to that of the electrodes in the furnace in question. Since the temperature and rate of erosion of the electrodes vary substantially with the size of the furnace and with the material being melted, the use of dielectric waveguides would necessitate individual selection of the ceramic cores at great cost.

From the above discussion it is clear that the hollow waveguide offers a significant cost advantage over the dielectric waveguide, while being the

simpler of the two to implement. The hollow waveguide has therefore been chosen as the guiding structure to be placed in the electrode.

3.2 Frequency of Operation and Waveguide Dimensions.

Common RF oscillators (GUNN and YIG oscillators), are available with operating frequencies in the *X-band* (8GHz-12GHz). The network analyser to be used for testing is able to measure frequencies up to 12.4GHz, therefore setting an upper limit. For reasons of availability and convenience, the operating frequency will be centered around 10GHz. The rest of the system must therefore be designed around this frequency.

The choice of cross-sectional shape is related more to the practical implementation of the system than to the theory of waveguides. The sections of waveguide used will be joined together as the electrode is slipped. A cylindrical waveguide would be the easiest to align and connect together during the joining phase. Cylindrical pipe is available cheaply in many sizes, and would be ideal as a waveguide. It was therefore decided to use cylindrical rather than rectangular waveguide.

The transmission media determines the basic form of energy which is to travel through it. If we were inserting a coaxial cable into the electrode, then TEM [4, page 16] (Transverse Electromagnetic) waves would be propagated. We are however using a waveguide, and are therefore restricted to TE (Transverse Electric) or TM (Transverse Magnetic) modes of propagation.

The various modes of TE and TM propagation are designated as TE_{mn}, where m and n are integers specifying various modes. Certain of these modes propagate in rectangular waveguides, and certain in cylindrical waveguides. Figure 3.1 shows the electric and magnetic field pattern in various rectangular and circular waveguides. For a full background on waveguides and transmission of electromagnetic waves, see [7, 11, 4]. Results derived in these texts will be quoted, and basic explanations given. However, derivations will not be provided.

The various modes of TE and TM waves can only exist in waveguides with certain cross-sectional dimensions. There is a minimum frequency called the *cut-off* frequency which can be propagated in a waveguide with given dimensions. Table 3.1 shows the *cut-off* frequencies for various modes in a circular waveguide with a diameter of 2cm.

When one designs a waveguide to propagate a certain mode, the dimensions

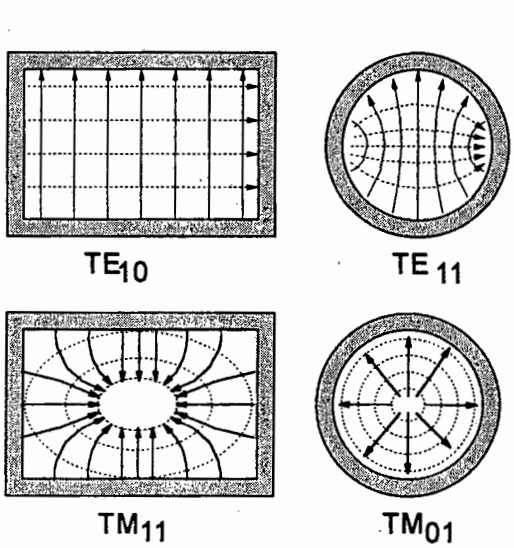

Figure 3.1: Electric and magnetic field patterns in guiding structures.

Mode	formula for cut-off	cut-off freq (GHz)
TM_{01}	$\frac{c}{2.613 \cdot a}$	11.48
TM_{11}	$\frac{c}{1.640 \cdot a}$	18.29
TM_{21}	$\frac{c}{1.224 \cdot a}$	25.51
TE_{01}	$\frac{c}{1.640 \cdot a}$	18.29
TE_{11}	$\frac{c}{3.412 \cdot a}$	8.792
TE_{21}	$\frac{c}{2.057 \cdot a}$	14.58

Table 3.1: Cut-off frequencies for a steel tube of diameter 2cm (GHz)

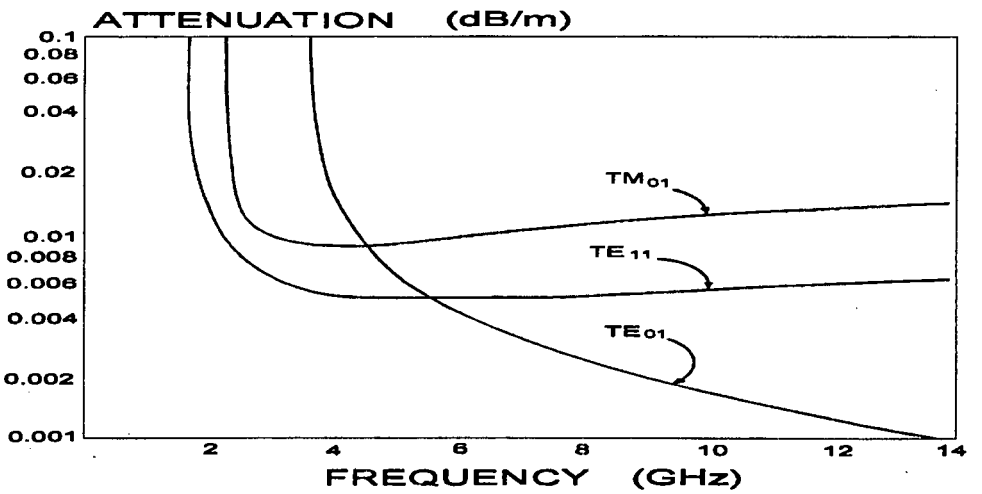

Figure 3.2: Attenuation of circular modes in copper waveguide.

of the waveguide must be such that the carrier frequency is higher than the cut-off frequency for that particular waveguide.

Figure 3.2 shows the attenuation per metre of various modes in a cylindrical copper waveguide. From Figure 3.2 we see that at higher frequencies the attenuation per metre of TE_{01} mode propagation drops off sharply. The reason for this is as follows. The mechanism of attenuation in a waveguide is the resistance of the waveguide walls. As the wave travels along the waveguide, the electric field couples into the waveguide walls, and power is dissipated in the form of heat in the same way that a current flowing through a resistor dissipates heat. Since the power dissipated in the waveguide walls is related to the density of the electric field being coupled into the walls, those modes which have a low density of electric field lines near the boundaries of the waveguide, experience less attenuation. Theoretically the TE_{01} circular mode has no electric field lines near the waveguide boundaries at high frequencies, and therefore suffers little attenuation.

The physical dimensions of the waveguide must now be determined. Since the different modes of propagation travel at different velocities along the waveguide and cause ambiguous measurements, it is advantageous to have pure modes propagating down the waveguide. Pure modes must therefore first be launched, and then maintained. In addition to causing attenuation, irregularities in the waveguide walls cause reflections of the propagating wave, which may give rise to mode conversion. In other words, modes are created by reflection which are different from the modes which were launched, and this causes ambiguous measurements. Mode filters can

Mode	diameter (cm)		
	1	2	4
TM_{01}	22.96	11.48	5.74
TM_{11}	36.59	18.29	9.14
TM_{21}	49.02	25.51	12.25
TE_{01}	36.59	18.29	9.14
TE_{11}	17.58	8.792	4.39
TE_{21}	29.17	14.58	7.29

Table 3.2: Cut-off frequencies (GHz) for circular waveguides of different size

be installed into the waveguide at regular intervals. However, these are impractical for an electrode-length-measurement system.

One way to ensure pure mode propagation is to make sure that the mode which was launched is the only mode which can exist in the waveguide. Table 3.2 shows the cut-off frequencies of various modes in waveguides with different radii. As can be seen from the table, if a 1cm diameter waveguide is used at 10GHz, none of the modes will propagate. If a 4cm diameter waveguide is used, all the modes except TM_{21} will propagate. A 2cm diameter pipe allows only the TE_{11} mode to propagate. So if a 2cm diameter pipe was used, pure TE_{11} mode would propagate, and no mode filter would be necessary to ensure unambiguous measurements. It is common practice to operate a waveguide above its cut-off frequency, so the diameter of 2cm could be increased slightly if necessary.

TE_{11} mode is also the easiest mode to launch into a waveguide. So although, as can be seen from Figure 3.2, TE_{11} mode offers slightly more attenuation per metre than TE_{01}, TE_{11} was chosen as the mode to be propagated down the electrode due to the ease with which it can be launched and maintained as a pure mode.

The waveguide is therefore to be cylindrical with an inner diameter of 2cm (or slightly more if necessary) to ensure pure mode propagation and unambiguous measurements. A stainless steel pipe with an inner diameter of 2.2cm was used for all further experiments due to availability.

3.3 Techniques of Launching Electromagnetic Energy Into the Waveguide.

TE_{11} mode electromagnetic energy has been chosen to be propagated down the electrode. A rectangular waveguide launcher (Figure 3.3) is used to produce TE_{10} rectangular mode electromagnetic energy. In order to convert this mode to TE_{11} circular, the rectangular waveguide can simply be placed end-on-end with a circular waveguide. This is due to the fact that the electric and magnetic field lines in TE_{10} mode rectangular and TE_{11} mode circular line up, as can be seen in Figure 3.1. This technique is however inefficient since not much TE_{11} mode energy is coupled into the circular waveguide. Three possible techniques for maximising the power coupled into the circular waveguide will be considered.

- Direct coupling between rectangular and circular waveguide
- A tapered rectangular-to-circular waveguide transition
- A tapered rectangular-to-circular waveguide section including matching screws

Direct coupling is the technique mentioned above in which rectangular waveguide is simply attached to circular waveguide. The inefficiency of this method is due to the impedance mismatch between the rectangular and circular waveguide sections. This impedance mismatch results in a significant proportion of the transmitted energy being reflected at the transition point, and not being coupled into the pipe.

A tapered rectangular-to-circular waveguide transition presents a gradual impedance change from the circular to rectangular waveguide, and therefore increases the coupling into the circular waveguide. The length of the taper should be $\frac{1}{4} + \frac{n}{2}$ wavelengths long to produce the best match at the center frequency (10GHz). The tapered transition can be further enhanced with tuning screws to match the two waveguide sections inductively.

The three methods were tested, and the results are shown in Figure 3.4. The measurements were made by launching energy into a rectangular waveguide with circular waveguide connected to it using the various techniques. Microwave absorbent material was placed at the end of the circular waveguide to minimise end reflections. The reflected power was then measured relative to the transmitted power (S_{11} reflection measurements).

As can be seen from the figure, the tapered section provides the best match at the center frequency, as expected. However, this match deteriorates

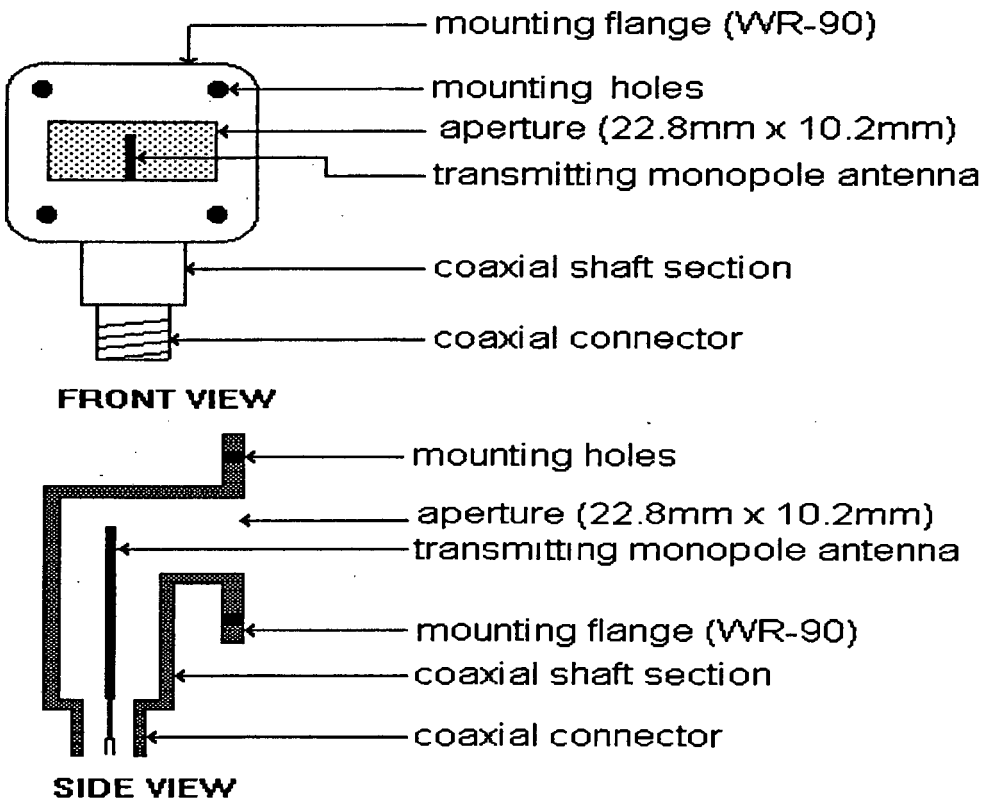

Figure 3.3: X-band (8-12GHz) TE_{10} mode launcher

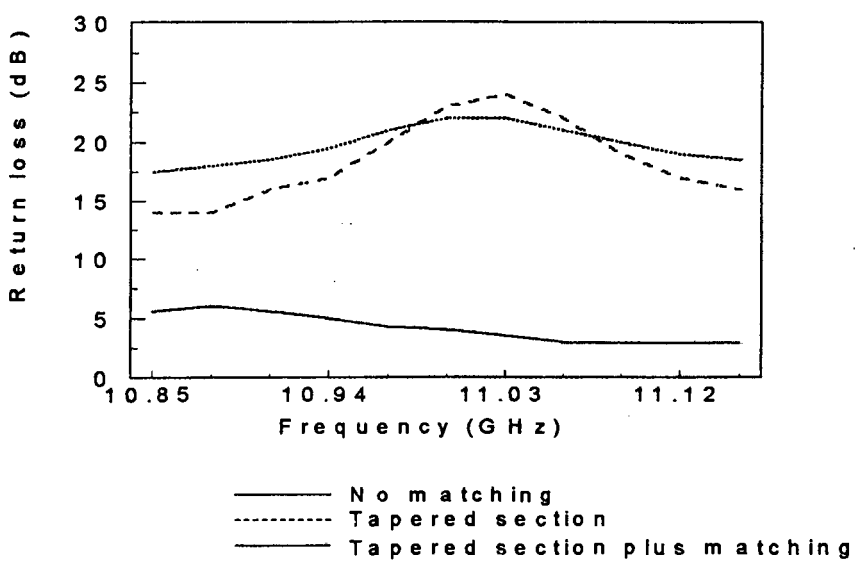

Figure 3.4: Measured attenuation of various TE_{11} mode launchers.

as one moves away from the centre frequency. The tapered transition with matching screws was chosen because it provides a good match across a wide band of frequencies. The design of the launcher is shown in Appendix A.

3.4 Group Velocity in the Circular Waveguide

In order to measure electrode length, the time taken for EM energy to reach the bottom of the electrode must be calculated. One of the radar techniques discussed in Section 4 will be used for this purpose. To convert the calculated time into a length measurement, the velocity of EM energy in the waveguide must be known.

The velocity at which EM energy travels in a waveguide is called the group velocity, and is given by [7, page 528]:

$$u_g = c\sqrt{1 - \left(\frac{f_c}{f_o}\right)^2} \tag{3.1}$$

The cut-off frequency (f_c) can be calculated from the relationship given in Table 3.1 for TE_{11} mode operation. It was found to be 8.99GHz in the 2.2cm diameter waveguide being used for investigation. The frequency of operation (f_o) is 10GHz, and the speed of light can be taken as the free space value since ϵ_r (relative permittivity) and μ_r (relative permeability) are both unity in the hollow waveguide.

The group velocity of TE_{11} circular mode in a 2.2cm diameter steel waveguide has been calculated in to be $180 \cdot 10^6$m/s. This is the velocity of EM energy which will be used in all further waveguide calculations.

3.5 Attenuation in the Steel and Graphite Waveguide sections

Each of the radar techniques to be considered for the measurement system relies on a similar principle: reflected microwaves are interpreted to determine distance. In an electrode measurement system, microwaves will have to propagate down an electrode and back up. It is important that the attenuation suffered by the microwave on its return trip should not be sufficiently large to prevent reception.

When microwaves are launched into an electrode, they will travel in a steel waveguide. The attenuation suffered in the steel waveguide will be negligible due to the high conductivity of the waveguide walls (see Section

3.2), and will be ignored. When the steel waveguide melts (above $\approx 800°C$), the wave must continue propagating in the resulting graphite-walled cavity. This is where the majority of attenuation will occur. Figure 2.3 shows the conductivity of graphite over a range of temperatures. One can see from this graph that the conductivity of graphite is above 20kS/m at temperatures above 800 °C. The approximate attenuation of TE_{mn} modes [4] in dB per metre is given by:

$$\alpha = \frac{8.686\sqrt{\frac{2\cdot\omega\cdot\epsilon_o}{\sigma}}}{2\cdot a\sqrt{1-\frac{{\omega_c}^2}{\omega^2}}}\cdot\left(\frac{p^2}{k^2\cdot a^2-p^2}+\frac{{\omega_c}^2}{\omega^2}\right) \tag{3.2}$$

where

- a is the diameter of the graphite waveguide section ($a = 0.022m$)
- ω is the frequency of operation in rad/s ($2\cdot\pi\cdot 10GHz$)
- ω_c is the cut-off frequency in rad/s ($2\cdot\pi\cdot 7.99GHz$)
- σ is the conductivity of graphite (20kS/m)
- ϵ_o is the permittivity of free space ($\frac{1}{36\cdot\pi\cdot 10^9}$F/m)
- k is the wave-number at the cut-off frequency, and is given by: $k = \frac{\omega_c}{c}$
- p is the mode number ($p = 1$)

From Equation 3.2, the attenuation of a circular graphite waveguide with a diameter of 2.2cm was found to be 1.76dB/m.

So, if the wave had to propagate down the last five metres of the electrode and back, $2\cdot 5m\cdot 1.76$dB/m=17.6dB attenuation would be realised. Since a typical microwave source can deliver 10 dBm, and a typical receiver can detect -90 dBm, a maximum attenuation of 100 dB can be tolerated. Other factors will however reduce this figure. 17.6dB attenuation in the graphite section is therefore large, but not prohibitive.

Unfortunately, it could not be determined at what frequency the conductivity measurements had been made, and since conductivity is dependent on frequency, the theoretical result could not be relied upon. Therefore, an experiment (Figure 3.5) was performed to determine the low-temperature attenuation of a section of graphite waveguide. Figure 3.6 shows the measured attenuation as a function of frequency. It can be seen from the figure that the measured attenuation ranges from 0.1dB/m to 0.8dB/m, and is therefore lower than the theoretical value. Heating the graphite waveguide

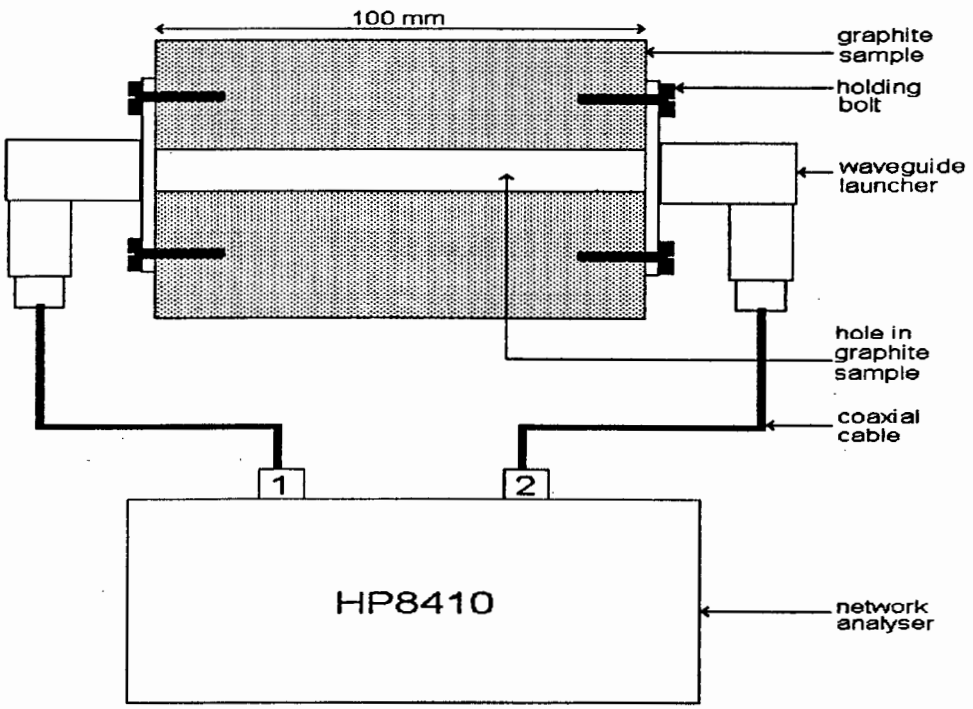

Figure 3.5: Apparatus used to find the attenuation of graphite waveguide.

to 265°C made no detectable change in the attenuation. At the physical position in the electrode where the wave would propagate in graphite, the temperatures are much higher than those in the experiment. The conductivity would therefore be greater, and the attenuation would be lower. If the attenuation of the graphite were found to be too large, then the diameter of the tube could be increased slightly; or alternatively, operation of TE_{01} mode instead of TE_11 mode propagation could be considered.

Other losses in the system would include:

- mismatches in the waveguide launcher, and in the transition between rectangular and circular waveguide
- reflections at the transition between the steel and graphite waveguide in the electrode
- attenuation of high frequency cables and connectors

The majority of these could, however, be kept low with good design and efficient implementation.

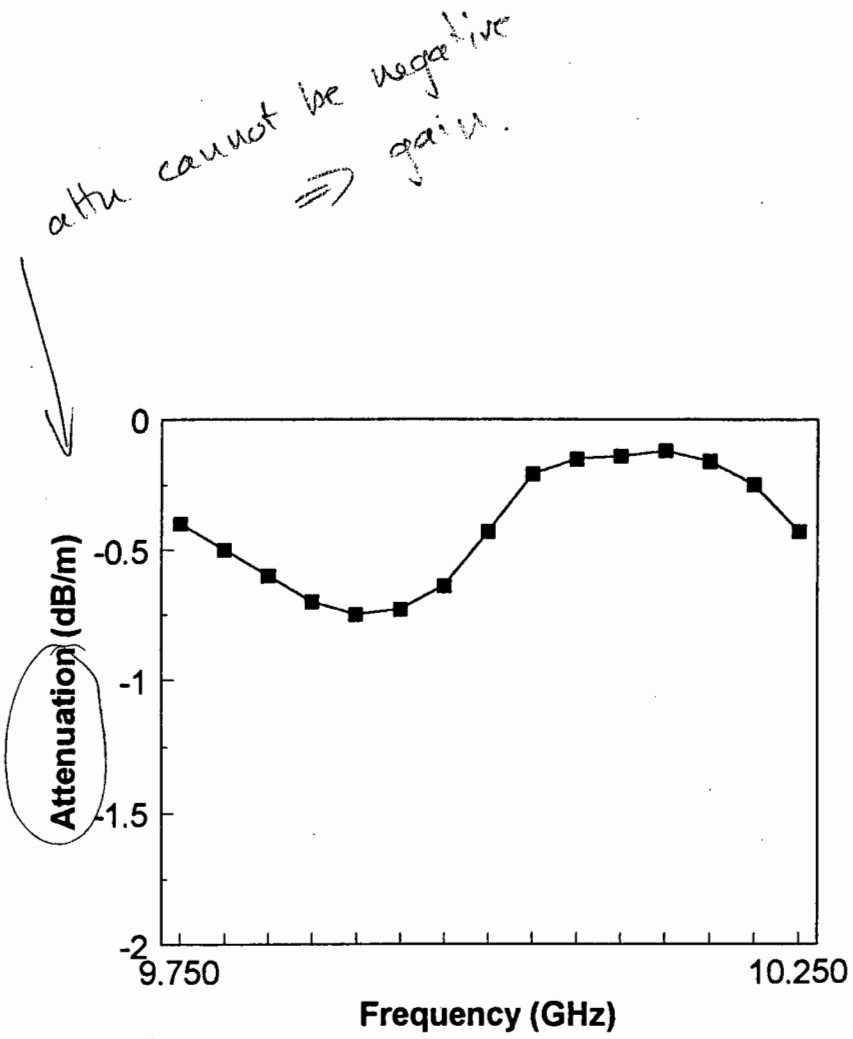

Figure 3.6: Attenuation of graphite waveguide as a function of frequency.

Chapter 4

RADAR SYSTEM DESIGN

There are various radar techniques which fall into the two broad categories of *pulsed radar* and *continuous wave radar*. Each of the two methods will be considered with reference to the electrode-length-measurement problem. A suitable radar will then be designed using the chosen technique.

4.1 A Pulsed Radar Measurement System

The principle used in a pulsed radar is that the time (t) taken for a single pulse to be transmitted, reflected by a target and received is measured. The distance to the target, or the length of the electrode (R) is then given by Equation 4.1, [13, page 109]:

$$R = \frac{u_g \cdot t}{2} \tag{4.1}$$

where u_g is the group velocity in the waveguide (electrode), and the factor of a $\frac{1}{2}$ accounts for the measured time representing the full return time to and from the target. In practice, a train of pulses as shown in Figure 4.1 would be transmitted.

The time between pulses is set so that the transmitted pulse has had time to return before a new one is sent. The maximum range of a pulsed radar is therefore set by the time between pulses, or the rate at which pulses are transmitted (pulse repetition frequency or PRF).

For the electrode measurement system, the maximum length of the electrode is assumed to be 20 metres. From Section 3.4, the velocity of energy transmission (group velocity) is known to be $180 \cdot 10^6$m/s. The maximum

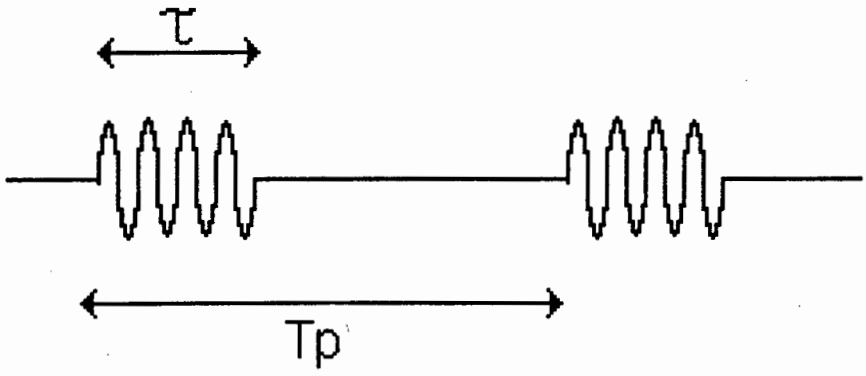

Figure 4.1: Train of radar pulses.

PRF is given by [13, page 110] as:

$$PRF = \frac{u_g}{2 \cdot R} \tag{4.2}$$

So the maximum PRF for the electrode measurement system would be 4.5MHz which means that 4.5 million electrode-length measurements could be made per second. However, a few measurements per second would suffice.

It can be shown that the resolution of a pulsed radar system depends on the width of the transmitted pulse, with higher resolution being obtained with narrower pulse widths (τ). The range resolution is given by:

$$\Delta R = \frac{u_g \cdot \tau}{2} \tag{4.3}$$

In order to obtain the high resolution required in the electrode measurement system, a very narrow pulse width is required. For 5cm range resolution, the pulse width needs to be 490 picoseconds, which is extremely narrow. The approximate bandwidth of the system required to transmit and receive such a pulse is given in hertz by the inverse of the pulse width in seconds, and is found to be 2GHz. This may be realisable if the transmission medium were free space, as is the case with most radars. The bandwidth of the waveguide, which is the transmission medium in this case, should be kept as low as possible to prevent dispersion, and to ensure single-mode propagation.

The high bandwidth of a pulsed radar system therefore makes it impractical for use in the electrode-length-measurement system; other methods will now be considered.

4.2 Multi-Frequency Continuous Wave Radar

Multi-frequency continuous wave (MFCW) radar is widely used in surveying equipment such as tellurometers. It is hoped that it will offer some advantages in an electrode-length-measurement system.

In MFCW radar, a high frequency signal is transmitted, reflected off a target, and received. The phase shift incurred during this journey is then measured to determine the distance travelled by the signal.

Range (R) as a function of phase shift (ϕ) is given by:

$$R = \frac{\phi \cdot u_g}{2(2\pi \cdot f)} \tag{4.4}$$

Unfortunately, the phase is ambiguous, having a period of 2π. Therefore, ranges of larger than half a wavelength ($\approx$1.5cm) will be ambiguous. This problem can be overcome if the phase shift due to more than one frequency is measured [9]. Equation 4.4 then becomes:

$$R = \Delta\phi \cdot \frac{u_g}{2 \cdot (2 \cdot \pi \cdot \Delta f)} \tag{4.5}$$

where Δf is the difference between the two measurement frequencies, and $\Delta\phi$ is the difference in measured phase. From Equation 4.5, the unambiguous range is found when ($\Delta\phi = 2 \cdot \pi$) or:

$$R_o = \frac{u_g}{2 \cdot \Delta f} \tag{4.6}$$

A system must therefore be built that can be used to measure the phase difference between two high-frequency signals. There are various well-documented systems, which can be broken down into two main categories:

- *Homodyne* or zero intermediate frequency (IF) systems
- *Superheterodyne* or non-zero IF systems

In zero-IF systems, phase difference is measured at high frequency, whereas in non-zero-IF systems, phase information is modulated down in frequency and measured at a standard intermediate frequency. This allows the use of high-quality, narrow-band amplifiers and filters, which results in improved noise performance. The superheterodyne receivers therefore offer improved performance when compared with homodyne systems. Figure 4.2 shows the system layout for a homodyne receiver, and Figure 4.3 the system layout for a superheterodyne system.

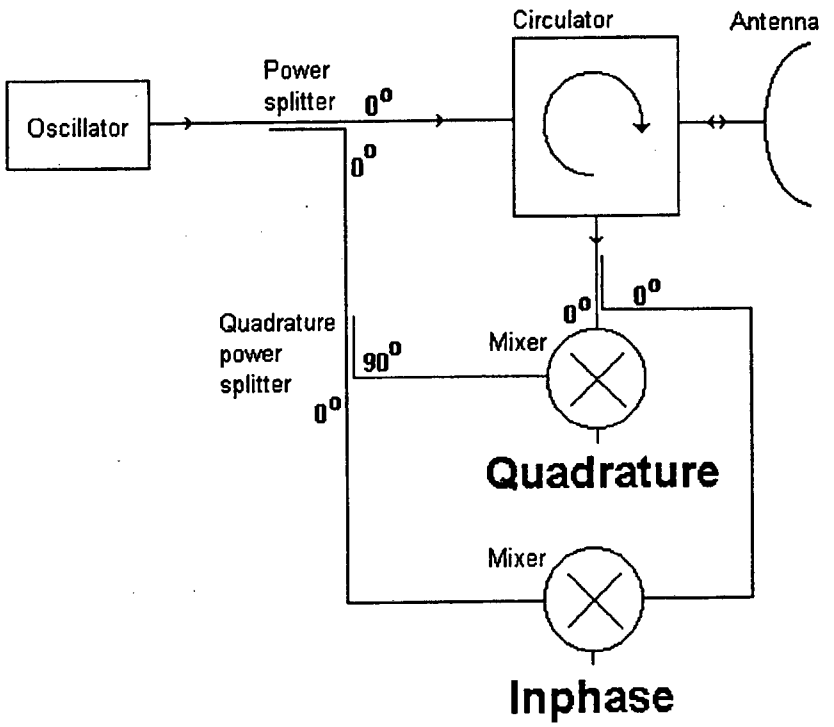

Figure 4.2: System layout for a homodyne system.

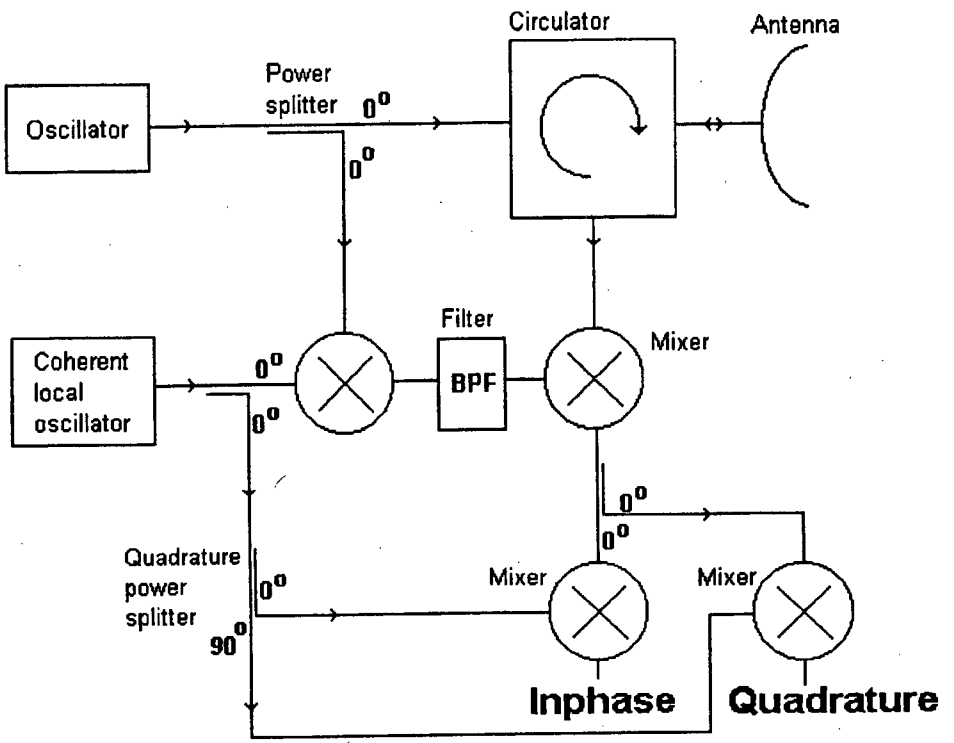

Figure 4.3: System layout for a superheterodyne system.

As can be seen from Figures 4.2 and 4.3, the superheterodyne system requires more hardware than the homodyne system.

Both systems use a similar principle. A signal is propagated down the electrode and reflected at the bottom. This reflected signal is then mixed with the transmitted signal to determine their phase difference. In practice, the received signal is mixed with in-phase and quadrature components of the transmitted signal. In this way, the *in-phase* (I) and *quadrature-phase* (Q) components are formed. The phase can then be calculated as:

$$\phi = \arctan(\frac{Q}{I}) \tag{4.7}$$

4.2.1 MFCW radar accuracy analysis

Partial differentiation of Equation 4.5 yields the range accuracy using MFCW radar:

$$\epsilon_R = \left|\frac{\delta R(\Delta\phi, \Delta f)}{\delta(\Delta\phi)} \cdot \epsilon_{\Delta\phi}\right| + \left|\frac{\delta R(\Delta\phi, \Delta f)}{\delta(\Delta f)} \cdot \epsilon_{\Delta f}\right| \tag{4.8}$$

From which we get the normalised range accuracy as:

$$\frac{\epsilon_R}{R} = \frac{\epsilon_{\Delta_\phi}}{\Delta\phi} + \frac{\epsilon_{\Delta f}}{\Delta f} \tag{4.9}$$

Where:

- R is the length of the electrode
- $\Delta\phi$ is the difference in measured phase at the two measurement frequencies
- Δf is the frequency difference between the two measurement frequencies
- ϵ_R, $\epsilon_{\Delta\phi}$ and $\epsilon_{\Delta f}$ are the respective errors in the above quantities

For an electrode length of 20m, a frequency span of 500MHz, a phase error of 5 degrees and a frequency span error of 100kHz, the range error is found using Equations 4.5 and 4.9 to be 6.5mm. This value is well within the system requirements.

4.2.2 Problems encountered with MFCW radar

Some simple tests were done using a system similar to that shown in Figure 4.2 to verify the principles used in MFCW Radar.

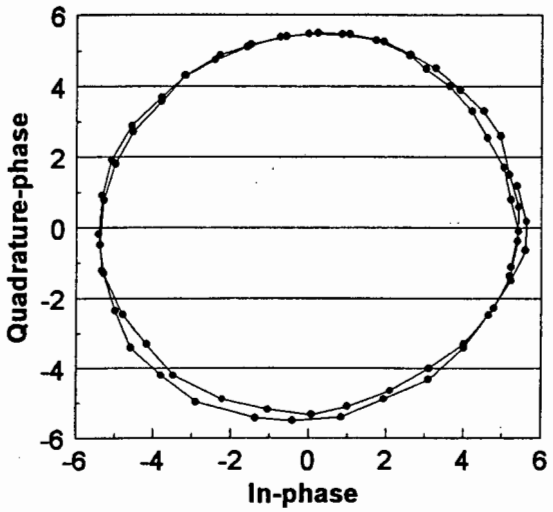

Figure 4.4: In-phase and quadrature-phase components plotted on orthogonal axes.

A reflective plunger was placed in a steel pipe, and microwaves were propagated down the pipe. As the plunger was pushed up the pipe, the in-phase and quadrature-phase components were expected to trace out sine and cosine functions, or a circle if plotted on orthogonal axes. A homodyne MFCW radar system was implemented to measure the phase components. The resulting phase was found to be inaccurate, and time-varying. After some experimentation, it was found that the microwave mixer was prone to DC drift over time, and that this drift was causing distortion of the phase components.

A heterodyne system overcame the temperature-drift problems associated with the mixer. The in-phase and quadrature components were once again plotted against each other, and the result is shown in Figure 4.4.

As can be seen from the figure, the shape of the graph is fairly close to that of a circle. Applying the phase measurements to Equation 4.5 gave an accuracy of approximately 10cm using this system.

There was however another source of error. The MFCW radar does

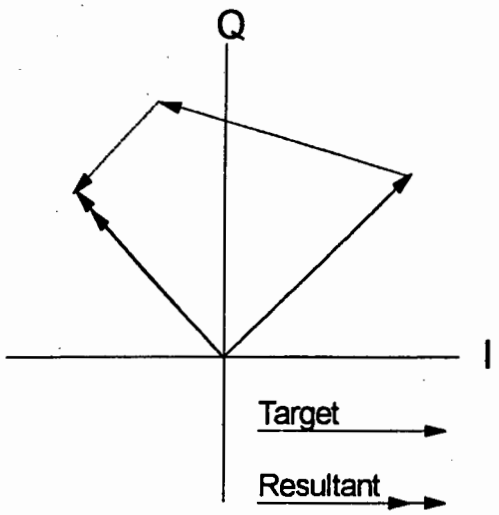

Figure 4.5: Multiple reflections found in a real MFCW system.

a vector measurement of the reflected wave (amplitude and phase). This vector will be made up of all the small reflections which occur along the pipe. Under laboratory conditions, these minor reflections would be static, and could be calibrated out. In the real system, however, there will be larger reflections (Figure 4.5), and they may be dynamic (e.g. the reflection from the transition between the steel pipe and the inner core of the electrode). So although the MFCW Radar offers excellent measurement accuracy in some cases, it cannot be used in an electrode-length-measurement system.

4.3 Frequency-Modulated Continuous Wave Radar

FMCW radar is used in aircraft altimeters and radar speed traps. It is one of the simplest and cheapest radars to implement, while being robust and reliable.

In an ideal FMCW radar, a linear ramp of frequencies as shown in Figure 4.6 is transmitted. The frequency difference at any instant in time between the transmitted and reflected signals determines the target range. The time delay between transmitted and received waveforms is given by:

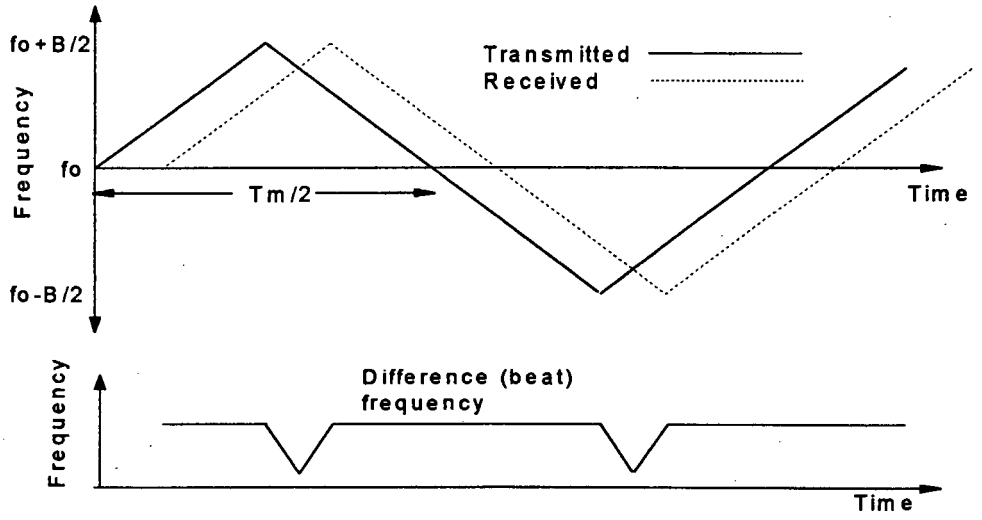

Figure 4.6: Linear frequency modulation to obtain range.

$$T = \frac{2 \cdot R}{u_g} \tag{4.10}$$

where u_g is the velocity of electromagnetic energy in the transmission medium.

The frequency difference between transmitted and received signals is called the beat frequency, f_b, and can be found from Figure 4.6 as:

$$f_b = T \cdot f' = \frac{2Rf'}{u_g} \tag{4.11}$$

where f' is the rate of frequency change, and is given by:

$$f' = \frac{B}{\frac{T_m}{2}} \tag{4.12}$$

where B is the maximum frequency deviation and T_m is the period of the modulation. The modulation frequency (f_m) is given by $\frac{1}{T_m}$.

Using Equations 4.11 and 4.12, we get an expression for range as:

$$R = \frac{u_g \cdot f_b}{4 \cdot B \cdot f_m} \tag{4.13}$$

The values of f_m and B can be chosen once the range and beat frequency have been selected. In the case of the electrode-length-measurement radar, the range R falls within the range 5m to 20m. The beat frequency will depend on the type of FMCW radar being implemented. The bandwidth (B) should be maximised, since it determines the resolution of the radar.

4.3.1 FMCW radar accuracy analysis

The range resolution (ΔR) can be found by taking partial derivatives of Equation 4.13:

$$\epsilon_R = \left|\frac{\delta R(f_b, f_m, B)}{\delta f_b} \cdot \epsilon_{f_b}\right| + \left|\frac{\delta R(f_b, f_m, B)}{\delta f_m} \cdot \epsilon_{f_m}\right| + \left|\frac{\delta R(f_b, f_m, B)}{\delta B} \cdot \epsilon_B\right| \tag{4.14}$$

Simplifying Equation 4.14 gives:

$$\epsilon_R = \left(\frac{\epsilon_{f_b}}{f_b} + \frac{\epsilon_{f_m}}{f_m} + \frac{\epsilon_{f_B}}{B}\right) \cdot R \tag{4.15}$$

From Equation 4.15, we see that the only way to increase the resolution is to decrease the percentage error in each measurement. For a range of 15m and a resolution of 5cm, the percentage error allowed for each parameter is only about 0.1%. This is a stringent requirement which will necessitate investigation into various error-reducing techniques.

Although the error requirements associated with the FMCW radar are stringent, they should be realisable. Furthermore, since in FMCW radar, a reflection is represented by a frequency output proportional to its distance from the radar, any spurious reflections can simply be filtered out. So an FMCW radar system provides target differentiation and does not require calibration as did the MFCW radar. In addition, the FMCW radar allows a large degree of freedom when choosing system parameters. For these reasons, it was decided to use FMCW radar, in conjunction with a waveguide inserted into the electrode, as the electrode-length-measurement technique to be investigated further.

4.3.2 The two types of FMCW radar

There are two main methods of implementing an FMCW radar. The first method will be termed *conventional FMCW radar*, and the other method *phase-locked-loop FMCW radar*. Block diagrams of the two methods will be shown, and their various merits discussed. Looking at Equation 4.13, one sees that the range is dependent on the beat frequency, the modulation frequency and the frequency deviation. So, in principle, any two of the three dependent variables could be kept constant. A measurement of the third variable would then provide the information to determine the electrode length. For practical reasons, the frequency deviation is always kept constant, and either of the other two variables is measured to determine range. When the beat frequency is measured to determine range, we call

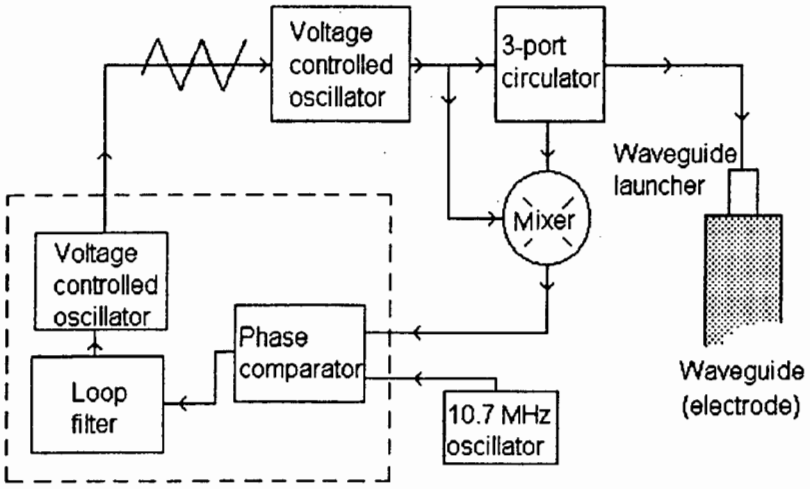

Figure 4.7: Phase-locked-loop implementation of an FMCW radar.

the radar a *conventional FMCW radar*, and when the modulation frequency is the measured variable, we have a *phase-locked-loop radar.*

4.3.3 Phase-locked-loop FMCW radar

In a *phase-locked-loop* (PLL) FMCW radar, the beat frequency is maintained using a PLL by changing the modulation frequency. The inverse modulation frequency is then measured to determine target range.

Advantages of PLL FMCW radars include:

- The hardware required is fairly simple and cheap.
- A PLL could track a very noisy beat frequency accurately.

4.3.4 Conventional FMCW radar

In conventional FMCW radar, the beat frequency is measured directly to determine target range. Various techniques, ranging from frequency counters to spectrum analysers and signal processing techniques, can be used to measure this frequency. Figure 4.8 shows a conventional FMCW radar system.

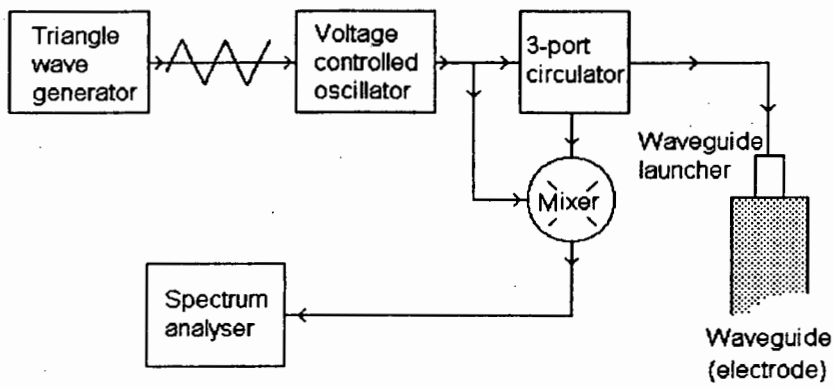

Figure 4.8: Conventional FMCW radar.

Advantages of the conventional FMCW radar include:

- The system is easy to interface to a digital computer.
- Complex signal processing can be done on the beat frequency spectrum if necessary, making the system robust
- The modulation frequency remains constant. This makes linearising a microwave VCO easier if it is found necessary.
- It is conceptually easier to understand than the PLL FMCW radar, and easier to implement.
- The beat frequency is directly proportional to target range.

4.3.5 The effects of nonlinear modulation on FMCW radar

All the radar equations rely on the components within the system being linear. It can be seen from Figure 4.9 that the tuning characteristic of a GUNN voltage controlled oscillator (VCO) is nonlinear, and therefore the equations do not strictly apply. The standard approach is to linearise the oscillator digitally. However, Skolnik [9, page 84] mentions that any periodic waveform can be used in an FMCW radar, and that the range is then given by the average beat frequency over a modulation period. Skolnik's approach

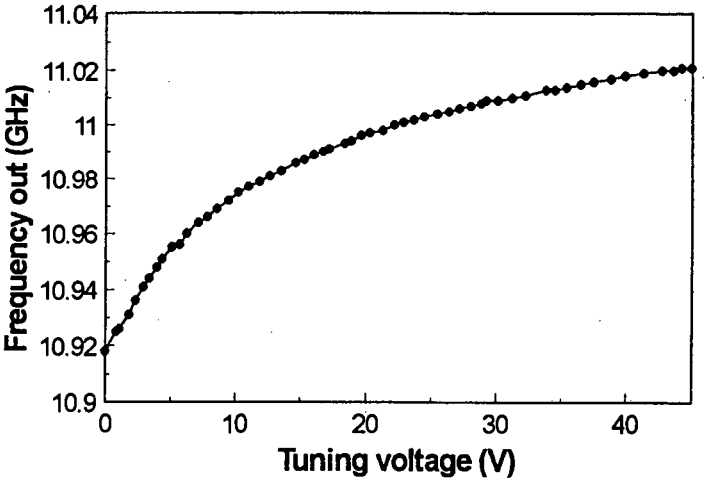

Figure 4.9: Voltage tuning characteristic for a GUNN oscillator.

will be investigated in this section before any digital solutions are considered. If the linearity is found to be crucial, a YIG (Yttrium Iron Garnet) oscillator with high linearity could be used. However, the YIG oscillators are expensive and will be avoided if possible.

The phase-locked-loop (PLL) implementation relies on the PLL being able to lock onto the beat frequency and keep it constant. This requires that the beat frequency be clearly distinguishable from any additional harmonics that might be present due to nonlinearities in the system. A conventional FMCW radar measures the beat frequency directly as a measure of range. Although digital signal processing can be used to enhance the beat frequency, the resolution obtainable will ultimately depend on the available *signal to noise ratio*. So if nonlinear modulation is to be used, the spectral purity of the beat frequency needs to be investigated. Secondly, it was found in Section 4.2 that target differentiation is necessary. In a linear FMCW radar system, different targets give rise to different beat frequencies and can be differentiated; the unwanted frequencies due to reflections other than from the target can simply be filtered out. It must be ensured that if nonlinear modulation is to be used, the spectral components from different targets do not overlap, or target differentiation will no longer be possible.

As mentioned before, an ideal FMCW radar would transmit a continuous linear frequency sweep. The frequency difference at any instant in time between the linear sweep and a delayed version results in the constant beat frequency. As a first look into the effect of nonlinearity, we can see that if the transmitted signal were not an exact delayed replica of the reflected signal, there would be small deviations in the difference between the two frequencies and hence in the beat frequency. The beat frequency would therefore no longer appear as a single spectral line, but would have a smeared frequency distribution.

A real FMCW radar could at best transmit a sawtooth or triangularly-modulated waveform. Figure 4.6 shows a triangularly-modulated signal, a delayed version and the resultant beat frequency. Since the beat frequency is the difference between the transmitted signal and a delayed version, triangular dips are seen to occur at the peaks and troughs of the modulation. One would therefore expect the beat frequency spectrum to contain a strong component representing the distance to the target. In addition, there would be harmonics at twice the modulation frequency centered around this main frequency.

Since the signal spends most of its time at the beat frequency, the power contained in this frequency component would be far larger than that contained in the harmonics due to the triangular dips. However, with increasing nonlinearity in the modulation, increased spectral power would occur in the harmonics.

These ideas were tested by simulating an FMCW radar with the program *Mathcad*. The modulation used took the form of a ramp with a varying nonlinearity added. Equation 4.16 was used to create the modulation.

$$y(x) = \frac{1}{a+b}(ax + bx^2) \qquad 0 < x < 1 \qquad (4.16)$$

The factor $\frac{1}{a+b}$ was necessary to keep the bandwidth (B) of the frequency sweep constant. With reference to the equation, nonlinearity was defined as $\frac{b}{a}$, so that 100% nonlinearity corresponds to $a = b$. Figure 4.10 shows the modulating sawtooth wave with 0% nonlinearity and 100% nonlinearity.

Figure 4.11 shows the beat frequency spectra for 0%, 5%, 10% and 20% nonlinearity. As can be seen from the figure, the linearity of the modulation is crucial to obtaining a clean, easily discernible beat frequency. In order to describe and quantify the effects of nonlinearity, two terms must be introduced. The *signal-to-spurious ratio* is defined as the average power in the beat frequency divided by the average noise or spurious output power, and

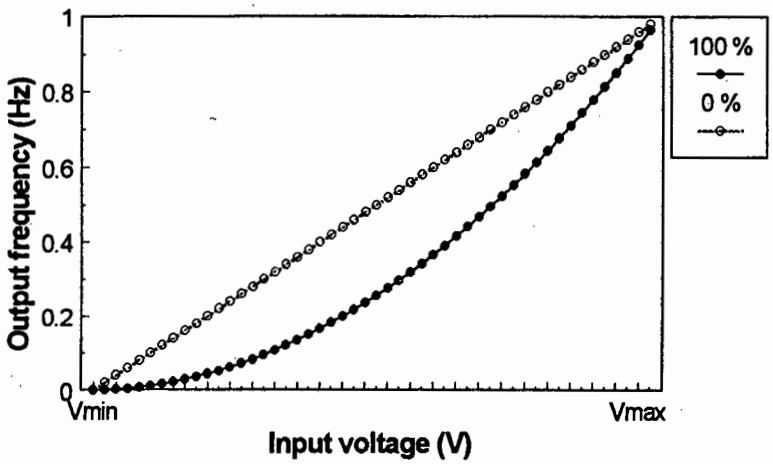

Figure 4.10: Modulation at 0% and 100% nonlinearity.

can be given in dB as:

$$\frac{\text{signal}}{\text{spurious}} = 10 \cdot \log\left(\frac{\text{beat}}{\text{noise}}\right) \tag{4.17}$$

The *bandwidth* is defined as the 3dB bandwidth in the standard manner.

The *signal-to-spurious* ratio and the *bandwidth* were measured for nonlinearities ranging from 0% to 100%. As can be seen from Figure 4.12, there is a strong dependency on the nonlinearity factor. A form of *quality* factor which is given by the *signal-to-spurious* ratio divided by the *bandwidth* is plotted in Figure 4.13.

The accuracy of the distance measurements which can be obtained with an FMCW radar is directly related to how accurately the beat frequency can be measured. A signal with a high *signal-to-spurious* ratio and low bandwidth can be measured far more accurately than one with a low *signal-to-spurious* ratio and high bandwidth. It can therefore be seen that to obtain accurate measurements from an FMCW radar, the modulating source has to be highly linear.

A quadratic regression to the GUNN tuning curve showed that it exhibits a 61% nonlinearity factor. The GUNN oscillator would therefore have to be

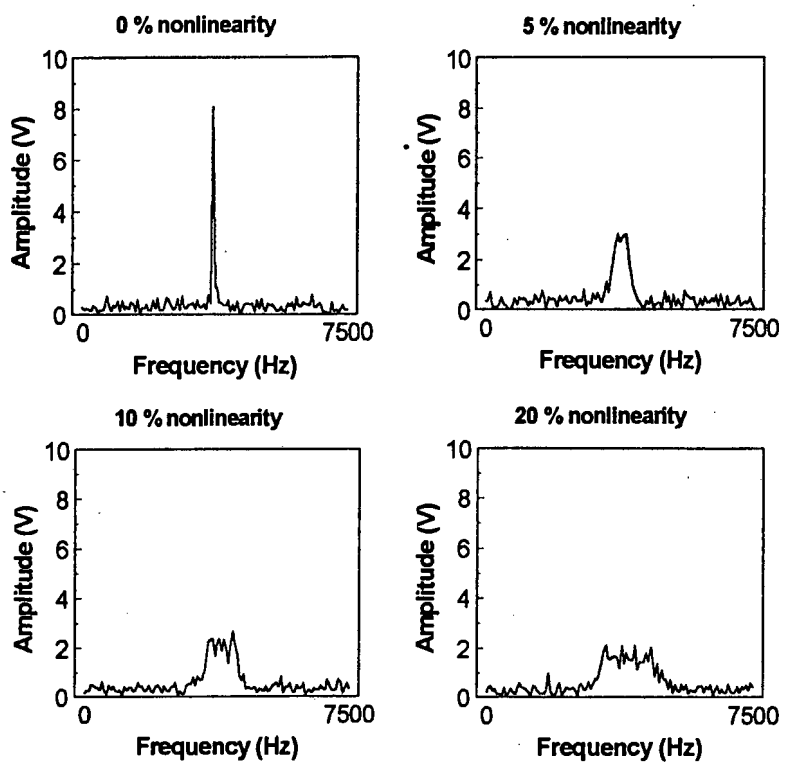

Figure 4.11: Beat frequency spectra at 0%, 5%, 10% and 20% nonlinearity.

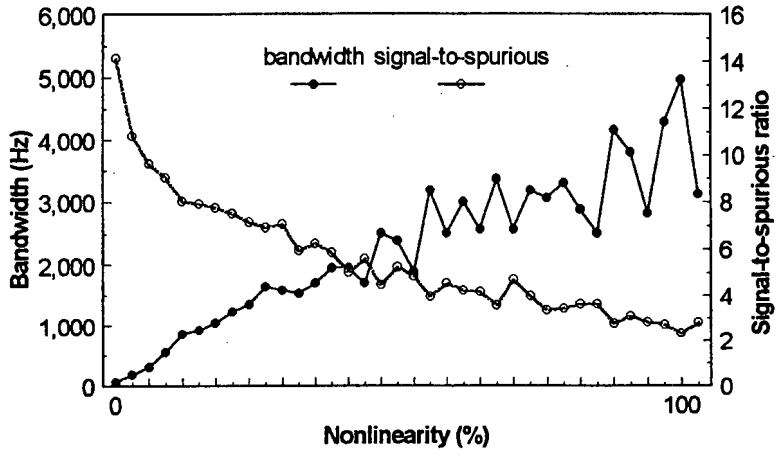

Figure 4.12: Signal-to-spurious ratio and bandwidth as a function of nonlinearity.

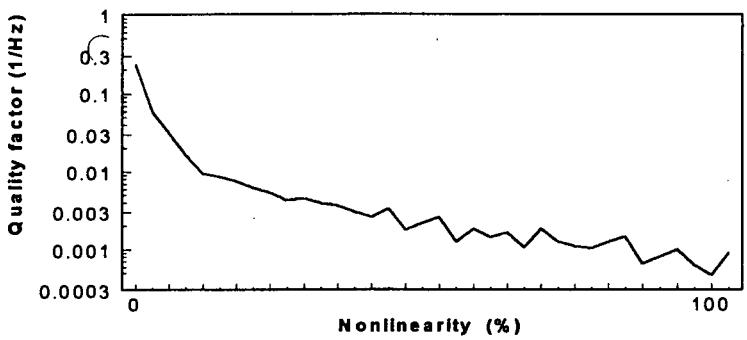

Figure 4.13: Quality factor as a function of nonlinearity.

linearised if either a PLL or conventional FMCW radar system were to be used.

4.3.6 A comparison between the two systems

It would do the averaging mentioned before.

The PLL FMCW radar offers simple, cheap hardware and the ability to track a fairly noisy beat frequency signal. The problem, however, occurs when the beat frequency becomes smeared due to nonlinearities in the system or because of multiple targets. At this stage some 'intelligence' would be of great advantage. The FMCW radar's compatibility with digital computers, and the consequent ability to perform signal processing, give rise to a versatile and robust system. In addition, changes can be made to the operating of the system without a significant change in hardware being required.

The FMCW radar measurement system will have to operate in a harsh, unpredictable environment. Although PLL FMCW radar does offer significant advantages over conventional systems, the robustness of the conventional system makes it more suitable for this application.

Chapter 5

IMPLEMENTATION

In this chapter, the technical aspects of the implementation of the radar will be discussed. The hardware and software dedicated to signal processing will also be described.

5.1 Technical Details of the Implementation of the Conventional FMCW Radar

The conventional FMCW radar technique offers a large degree of flexibility that is not present in any of the other techniques discussed so far. Conventional FMCW radars such as those used in altimeters employ simple frequency counters to determine the beat frequency. However, an aircraft altimeter operates in a fairly predictable environment, where it is known that the land surface will be the major source of reflection. In a furnace, no such prediction can be made about the environment. A microprocessor linked to the radar would give the system a certain amount of 'intelligence', which will be necessary in the furnace environment. The electrode measurement system to be implemented will therefore consist of a conventional FMCW radar linked to a computer. The computer will have the dual task of providing input to the radar, and of analysing the radar output.

5.1.1 Conventional FMCW radar parameters

The various subcomponents of the radar system to be discussed are the microwave, analogue and digital sections (Figure 5.1).

For reasons that will be explained in the sections below, the parameters of the FMCW radar were chosen as follows:

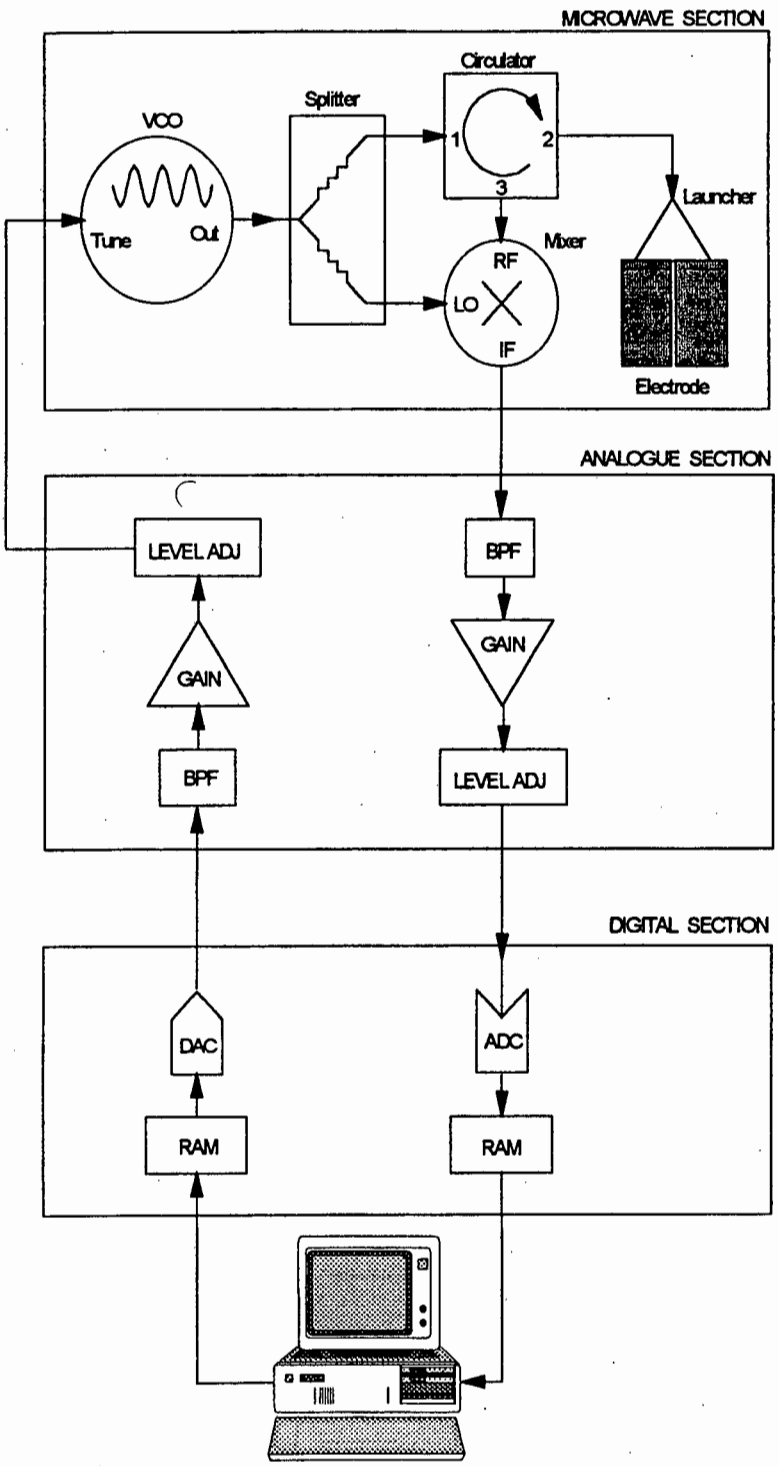

Figure 5.1: Schematic representation of electrode-measurement system.

Centre frequency	10GHz
Sweep bandwidth	500MHz
Modulation frequency	60Hz
Modulation type	sawtooth

Table 5.1: System parameters

The high-frequency component of the measurement system

A high-frequency voltage controlled oscillator (VCO) with a centre frequency of 10GHz (Section 3.2) acts as a microwave source. Radar resolution is known to be inversely proportional to bandwidth, as will be shown later in Equation 5.6. The bandwidth must therefore be maximised, while remembering that higher bandwidth results in greater waveguide dispersion. It was found experimentally that a bandwidth of 500MHz resulted in the best overall system performance. The various VCOs investigated were:

Manufacturer	Model no.	Frequency range (GHz)	Cost (R)
Avantek	VTO8950	9.5GHz - 10.5GHz	4095
Avantek	AV74010	8.0GHz - 12.4GHz	14000
Hewlett Packard	HP8530b	0.1GHz - 14GHz	20000

Table 5.2: VCO specifications

It was found in Section 4.3.5 that the microwave VCO linearity was crucial. The VTO8950 is a low-cost varactor-tuned oscillator with a nonlinear tuning characteristic that is temperature-dependent. It would therefore require temperature-dependent linearisation over the vast range of temperatures present in the furnace environment. Both The AV74010 (YIG) and HP8530b are temperature-stabilised and extremely linear. The HP8530b sweep oscillator was used because it was relatively easily available. However, in a practical version of the system, a YIG tuned oscillator would be substituted. The oscillator had a power output of 10dBm, which was flat across the system bandwidth. A regular power output is important to prevent harmonics due to amplitude modulation occurring in the beat frequency spectrum.

A 3dB Wilkinson power splitter delivered half the power to the mixer (7dBm), and half the power to the electrode through a TE_{11} mode waveguide launcher. An ordinary power splitter could have been used, but the Wilkinson power splitter has the advantage that it does not allow power reflected by mismatches in the system to pass back through the splitter. Reflected power arriving back at the oscillator causes an effect called *frequency pulling*,

Model number	MRI W-90 WJX-NC
Centre frequency	10GHz
Bandwidth	500MHz
Isolation	min 35dB
VSWR	max 1.3
Insertion loss	max 0.4dB
Waveguide type	WR-90
Flange type	UG 135/U

Table 5.3: Circulator specifications

during which the frequency of the oscillator can change substantially.

An X-band (8GHz to 12.4GHz) waveguide circulator was used. The measured isolation was above 34dB over the band 9.75GHz to 10.25GHz, and the insertion loss negligible. Table 5.3 gives the full specifications of the circulator.

A double-balanced mixer was used to find the difference in frequency between the transmitted and received signals because of its superior intermodulation product rejection capabilities [16]. The RF and LO inputs of the mixer covered the range of X-band frequencies, and the IF output was DC-coupled. It is important that the beat frequency should fall within the bandwidth of the IF output port. The LO input required an optimum of 6dBm to operate without producing excessive harmonics. If the power output of the VCO had been greater than 10dBm, a 3dB power splitter could not have been used because the LO port of the mixer would have become saturated and would then have produced harmonics. In this case, a directional coupler could be used to deliver optimum power to the LO port.

The waveguide launcher used has been described in Section 3.3.

The low-frequency analogue section of the radar.

The analogue circuitry used to interface the microwave and digital sections consists of amplifiers, gain sections and filters. All of these units were implemented using operational amplifiers, and some accompanying passive components. The details of each unit will not be given here, but the circuit diagrams are shown in Appendix B.

The beat frequency produced by the microwave mixer will contain unwanted harmonics and both high-frequency and low-frequency noise which must be filtered out. Because a sawtooth waveform instead of a triangular waveform is being used to modulate the microwave VCO, the definition given in Equation 4.12 becomes:

$$f' = \frac{B}{T_m} \tag{5.1}$$

The FMCW range equation is then given by:

$$R = \frac{u_g \cdot f_b}{2 \cdot B \cdot f_m} \tag{5.2}$$

Using Equation 5.2, it has been calculated that the beat frequency will fall into the range 1.7kHz to 6.7kHz depending on the length of the electrode (5m-20m). A 6th-order Chebyshev bandpass filter with a centre frequency of 4.2kHz and a bandwidth of 5kHz was therefore placed at the output of the mixer to attenuate unwanted harmonics and noise. Gain and offset sections were placed after the filter to optimise the signal levels before analogue-to-digital conversion. The input filter also prevents aliasing of the beat frequency signal due to sampling.

The computer produces the modulation for the VCO through a DAC. The output from the DAC is filtered to eradicate its stepped nature and then amplified and level-shifted to make it compatible with the input of the VCO. A simple low-pass filter in the feedback of the gain section provides the necessary smoothing.

Interface between the radar and the computer

The computer performs the dual task of sampling the output from the microwave section, whilst providing the modulation for the VCO. An interface between the radar and the computer to perform these tasks had to be designed and built.

Since a computer was to be used to sample the output from the radar, the beat frequency had to be kept fairly low. A lower beat frequency also means a lower modulation frequency, and this has the advantages of simplifying linearisation of the VCO, and of reducing capacitive effects on the tuning port. The modulation frequency was chosen as 60Hz, which, as mentioned before, results in a beat frequency of 1.7kHz to 6.7kHz, depending on electrode length.

In order to satisfy the Nyquist sampling theorem, the sampling rate must be at least twice the maximum beat frequency, or at least 13.3kHz. The sampling duration must be one period of the sawtooth modulation or 1/60Hz=16.7ms. The timing between samples must be extremely accurate, and must not be affected by system interrupts.

With reference to the microwave section of Figure 5.1: EM energy enters port 1 of the circulator, and should be directed through to port 2. However,

some of the energy 'leaks' through to port 3, and can be viewed as noise. The isolation associated with a particular circulator is its ability to isolate port 3 from port 1. Higher isolation results in less leakage and therefore a lower system spurious noise-floor. The system's ability to measure small reflections returning to port 2, or the system's *dynamic range* is therefore set by the isolation provided by the circulator. Although the specified isolation is 40dB, it has been measured to be more like 35dB. Since 7 bits provides 42dB dynamic range, a seven bit system would have provided the required 35dB dynamic range in this case; however, an eight bit system was chosen because of the computing standard.

An interface card with these specifications was therefore designed and built.

The steps involved in the operation of the interface card are:

- Calculate the modulation waveform using the computer;
- Apply a linearisation matrix to the modulating waveform;
- Load the modulation waveform into a memory on the interface card;
- Give the instruction for the card to start sampling;
- The interface then samples and outputs the modulation waveform at the same time;
- The interface tells the computer that it has completed sampling;
- The computer loads the sampled values from a memory on the interface into the computer;
- The computer analyses the beat frequency spectrum and determines the electrode length.

The interface has a high-speed DAC and ADC on board. There are two RAMs which are used to store the modulating waveform and the sampled data. Buffers isolate the computer from the card and therefore from the radar. An oscillator provides a clock which determines the sampling frequency. A counter, being incremented by the clock, logs data in and out of the RAMs. A full circuit diagram and timing diagrams are given in Appendix C. The final specifications of the interface card are shown in Table 5.4.

The corresponding curves for tests performed on the DAC and ADC sections of the interface are shown in Figure 5.2. An error analysis of the

Sampling frequency	62.66kHz
Sampling period	16.3ms
Number of samples	1024
Number of bits	8

Table 5.4: Interface card specifications

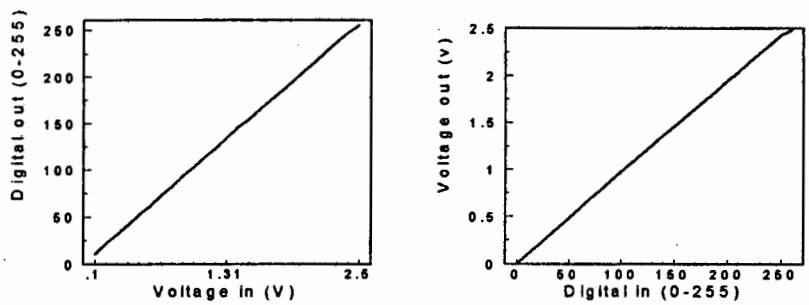

Figure 5.2: Linearity graphs for the DAC and ADC.

interface was undertaken, and the errors, which are defined by Horowitz and Hill [10, page 614-615] are shown in Table 5.5.

These errors are comparable to those reported by the manufacturers of the ADC and DAC chips. The guaranteed linearity set by National for the ADC (ADC0820) is 0.5 LSB. The final measured linearity of 0.43 bits is therefore within the limits specified by the manufacturer. National specifies the maximum linearity associated with the DAC (DAC0832) as 0.05% of the reference voltage or 0.00125 volts. The measured value of 0.006 volts compares well with this value. A source of extra error is that associated with stability of the power supply used as a reference for these experiments.

	Digital to Analogue Converter	Analogue to Digital Converter
	(volts)	(bits)
Linearity error	0.006	0.43
Scale error	0.00	0.20
Offset error	0.00	1.92

Table 5.5: Interface card error specifications

5.2 Signal Processing of the Radar Returns

Since the length of an electrode is proportional to the beat frequency, it is of extreme importance that the beat frequency be determined as accurately as possible. Traditionally, spectral estimation has been achieved using fast Fourier transforms (FFT). Although the FFT is able to provide quick and robust results, more modern techniques have been found which provide better frequency resolution. It was therefore decided to investigate some *modern* spectral-estimation techniques. *Mathcad* documents describing each of the techniques can be found in Appendix D.

The following spectral-estimation techniques were compared:

- Fast Fourier Transform (FFT)
- Prony's method
- Multiple Signal Classification (MUSIC) method

5.2.1 The fast Fourier transform

The FFT provides us with a computationally-efficient, reliable method of spectral estimation. There are however some inherent limitations associated with the FFT, the most prominent of these being the limit on spectral resolution i.e. the ability to distinguish two similar frequencies in a signal. According to the *Rayleigh criterion*, two signals should be considered to be just resolved when the first maximum from one component sits at the first minimum of the other [14, page 450]. Using the FFT, the obtainable resolution in Hz is approximately inversely proportional to the time in seconds over which the signal was sampled.

$$\Delta f = \frac{1}{T_s} = \epsilon_{f_b} \tag{5.3}$$

Therefore, if an FFT is used to analyse the beat frequency spectrum, the resolution with which the beat frequency can be determined will be given by the inverse of the sampling time. Assuming the modulation frequency error (ϵ_{f_m}) and the bandwidth error (ϵ_B) in Equation 4.15 to be negligible (this is reasonable, since with good hardware design they can be kept low), we obtain:

$$\epsilon_R = \frac{\epsilon_{f_b}}{f_b} \cdot R \tag{5.4}$$

or, substituting Equation 5.2 for R:

$\epsilon_R = \frac{180 \cdot 10^6}{2 \cdot 500 \cdot 10^6} = 18\text{cm}.$

$$\epsilon_R = \frac{\epsilon_{f_b}}{f_b} \cdot \frac{u_g \cdot f_b}{2 \cdot B \cdot f_m} \tag{5.5}$$

Then, by realising that $\epsilon_{f_b} = \frac{1}{T_s} = f_m$, it can be shown using Equation 5.3 that the range resolution obtainable when using an FFT is given by :

give a value for the situation here.

$$\epsilon_R = \frac{u_g}{2 \cdot B} \tag{5.6}$$

and represents resolution if one modulation cycle is used

where u_g is the velocity of the electromagnetic energy in the waveguide and B is the bandwidth of the transmitted signal in Hz. The aim of this chapter is to try to improve on the result obtained in Equation 5.6.

It is important at this point to introduce the signal processing terms *bias* and *variance*. The *bias* of a spectral estimator is the average error in the estimator. Therefore, a low *bias* gives an accurate absolute spectral estimate, as is required in this application. The *variance* of a spectral estimator is the mean-squared error associated with the estimator. A smooth curve has a low *variance* and a spiky curve a high *variance*. The higher the variance, the easier it is to differentiate two closely-spaced frequencies i.e. higher variance corresponds to better resolution. It must however be remembered that it is not resolution but absolute accuracy which is required in this application.

The first method of beat frequency estimation tested entailed squaring the magnitude of an FFT to obtain a *power spectral density*. The spectral component with the greatest amplitude was then taken as the beat frequency. Since the FFT is a discrete estimator, the beat frequency can only be determined to the nearest frequency bin in the estimator. Therefore, when using the FFT, the bias is limited to a minimum value of half the distance between frequency bins, or half the Rayleigh frequency. Averaging of the FFT spectrum decreases the bias slightly, but accuracy is rarely improved beyond the limit imposed by the Rayleigh criterion.

For means of resolution comparison, it was seen whether the various spectral-estimation techniques tested could resolve two sinusoids embedded in white noise. The frequencies of the sinusoids were 2Hz and 2.2Hz respectively, and the signal-to-noise ratio was 20dB. Figure 5.3 (a) shows that the FFT periodogram is unable to resolve the two frequencies due to its low variance.

5.2.2 Prony's method

The FFT assumes that a signal is composed of a set of harmonically-related sinusoids and it is therefore a discrete estimator. Prony's method is a tech-

nique for modelling data of equally-spaced samples using a linear combination of complex exponentials. Since the exponentials can have arbitary amplitude, phase and frequency, the spectral estimate becomes continuous and is no longer bound by the Rayleigh criterion.

The Prony method requires that the number of exponentials to be used in the model be known prior to spectral estimation. In cases where only an approximate fit to the data is required, the number of exponentials can be less than half the number of data points. In practice, however, far fewer terms are used in the model since the rough computational complexity is related to the squared power of the number of exponentials used in the model.

A complex rooting algorithm is required to determine the frequencies contained in the spectral estimate. This has the disadvantage of being computationally intensive, but it does produce results without having to search for maxima, as with the FFT. As can be seen from Figure 5.3 (b), the Prony method is well able to resolve the two sinusoids of 2Hz and 2.2Hz (see Appendix D for the *Mathcad* spreadsheet).

5.2.3 The MUSIC method

The MUSIC (*multiple signal classification*) [14] algorithm is an eigenvector-based projection approach to super-resolution spectral estimation. The basic idea is to partition the observation space spanned by the eigenvectors of a correlation matrix into two subspaces denoting signal-plus-noise and noise respectively. It can then be shown [14, page 454] that, under ideal conditions, the complex frequencies contained in the input data can be found from the subspaces. Under realistic conditions, spectral peaks in an approximate spectrum must be located.

The MUSIC method assumes prior knowledge of the number of complex sinusoids contained in the input data. The MUSIC algorithm was able to differentiate the two simulated sinusoids in Figure 5.3 (c).

5.2.4 Application to real data.

The three spectral-estimation techniques and some hybrids of them were tested on some real data that was measured using the FMCW radar system. Figure 5.4 shows a plot of a section of the radar return as measured using the system in Figure 5.1. Ideally one would expect a pure sinusoid as output from the radar. However, for reasons discussed in Section 4.3.5, this does not occur in practice. The measured result is seen to resemble a rough sinusoid,

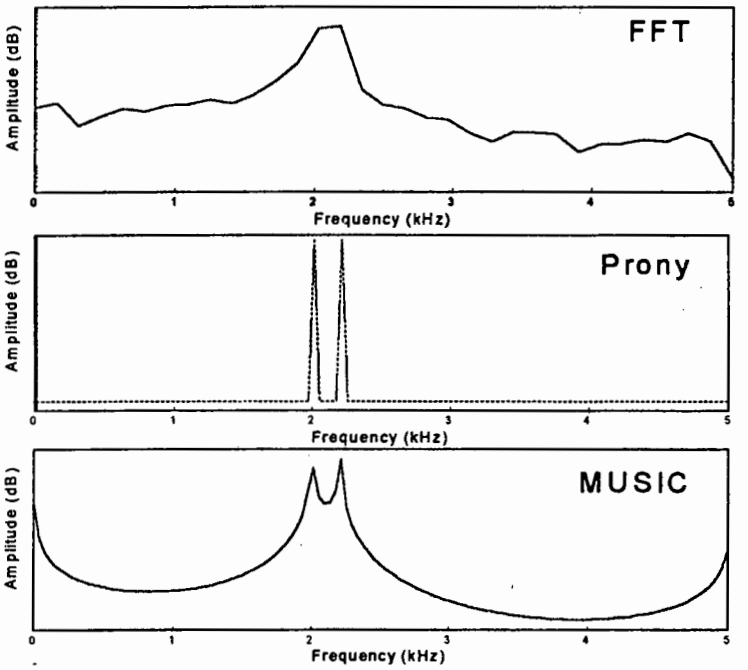

Figure 5.3: Spectral plots of simulated sinusoids at 2Hz and 2.2Hz.

as one would expect.

The three spectral-estimation techniques were applied to sets of sampled data taken at different electrode lengths. As can be seen from Figure 5.5, the three different methods worked with varying success.

Zero padding was applied to the FFT in order to smooth the result and to provide interpolation between the spectral bins. The figure shows that the FFT provides the most accurate absolute measurement of frequency, and therefore of length. Although the other spectral-estimation techniques provide better variance than the FFT, they tend to add a varying bias to the absolute measurement depending on the number of terms used in the model. This result agrees with [3, page 89] who mentions a trade-off between bias and variance. Table 5.6 gives a summary of the different techniques [15, page 1410] where N is the number of data samples and M is the order of the model used in the Prony and Music methods.

Therefore, on the grounds of its computational efficiency and robustness, the FFT was chosen as the spectral-estimation technique to be used to determine the beat frequency from the sampled FMCW radar data signal. As mentioned previously, zero padding was used to interpolate between values. A weighted average of a few spectral lines around the maximum also provided a simple means of further interpolation between spectral bins.

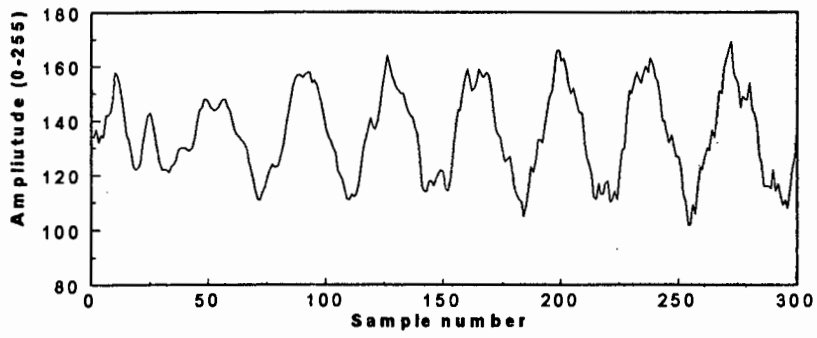

Figure 5.4: Section of the sampled output from the FMCW radar.

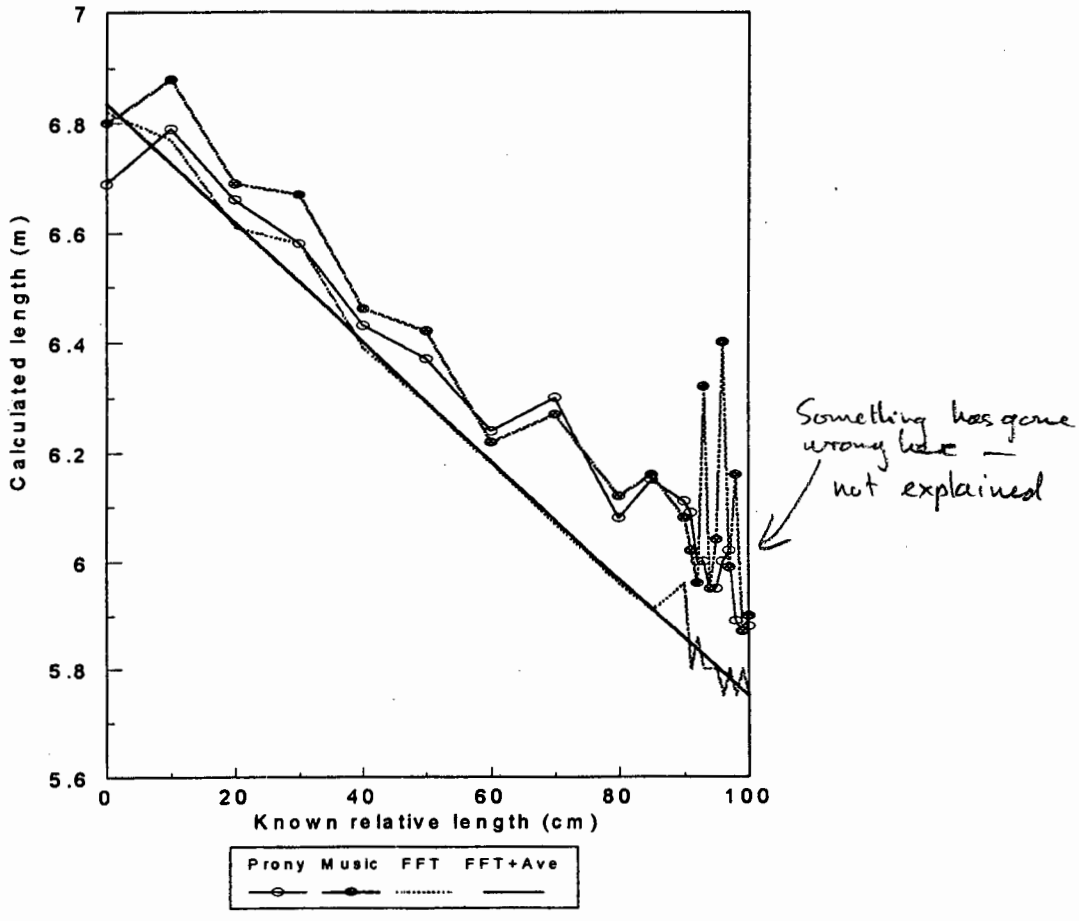

Figure 5.5: Length estimates as obtained using the three spectral-estimation techniques.

Technique	Discrete or Continuous	Complexity	Advantages and disadvantages
Fourier transform	D	$Nlog_2N$	Output directly proportional to power Most computationally efficient Resolution roughly the inverse of sampled time
Prony's method	C	$M^2 + MN$	Requires prior knowledge of order Requires polynomial rooting Resolution as good as autoregressive (AR) techniques Resolution exceeds that obtainable with FFT Requires high $\frac{S}{N}$ for low bias
MUSIC method	C	$M^2 + MN$	Requires prior knowledge of order Resolution exceeds that obtainable with FFT Requires high $\frac{S}{N}$ for low bias Sensitive to changes in spectral model

Table 5.6: Summary of the different spectral-estimation techniques.

The signal processing techniques as well as the data capture, the VCO linearisation and the interface card control procedures, were written in *Borland C*. The program, called RADAR, is listed in Appendix E.

flowchart would have been useful

Chapter 6

RESULTS

The FMCW-radar-based measurement system was set up as described in Chapter 5. A stainless steel pipe was used to represent the electrode, and a reflective plunger was inserted into the pipe to represent changes in electrode length.

The measurements were made using the HP3050 sweep oscillator as a frequency source, being swept by the *FMCW radar to PC* interface card. The results were logged by the interface card, interpreted by the PC and displayed as a length measurement on the PC display. Measurements were made over the approximate range 4.5m to 6.9m at one-centimetre intervals.

At first, only a simple FFT was used to determine the largest frequency component, and therefore the beat frequency could only fall into a discrete frequency bin. For this reason, the length measurements were stepped and not continuous as one might expect. Figure 6.1 shows a graph of measured length versus the known length. Although the stepped nature of the graph causes a large overall error, a linear regression showed that the gradient of the graph was almost ideal, having a slope of 1.001:1. Since the trend followed by the measurements was so accurate, but the overall accuracy was being limited by the discrete nature of the FFT (RMS error $\approx$ 7cm), it was decided to do some signal processing on the measured data. It should be noted that, for *absolute* measurements, the distance between the microwave components must be subtracted from the measured distance, but that for relative measurements this has no effect.

As mentioned in section 5.2, it was found that zero padding in conjunction with the FFT was the most successful signal processing technique. Weighted averaging was also found to improve the accuracy with which the beat frequency could be measured. This process was applied to the computer-based interpretation program, and the measurements were re-

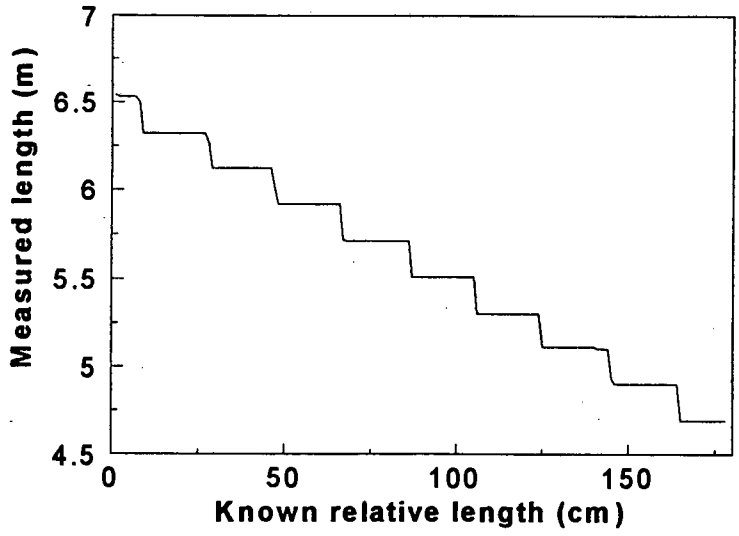

Figure 6.1: Length measurement with simple FFT signal processing technique.

peated. Figure 6.2 shows the repeated set of measurements. From the figure, it can be seen that the stepped nature of the measurements has been vastly reduced, but that accuracy has been maintained. When compared with the known length, it was found that the RMS error associated with the measurements was 1.37cm - well within the required limit.

Further measurements were then performed between eight and nine metres to determine whether the system was linear over large ranges. In order to perform these measurements, an extra section of pipe had to be added to the existing length. The discontinuity formed at the junction between the two pipes was found to have a very small effect. Alignment of the pipes was not critical to the performance of the system. The extended set of measurements lined up perfectly with the initial set (Figure 6.3), and proved that the system remains linear over extended ranges.

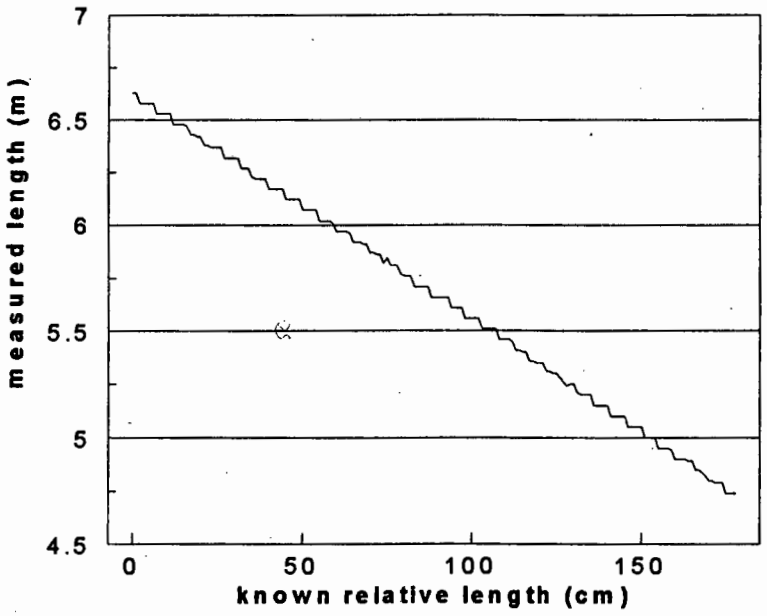

Figure 6.2: Length measurements with zero padding and a weighted average.

Finally, a 40cm thick section of Soderberg electrode was attached to the end of the pipe. The electrode had been pre-bored with an inner diameter equal to that of the pipe. Due to the crystalline nature of the electrode, the inner surface was rough, just as would be expected in a real application in a furnace. It was found that surprisingly little attenuation and virtually no wall reflections occurred in the section of electrode. The length-measurement system performed as well as in previous experiments, with the electrode section having no adverse effect on the measurements (Figure 6.4).

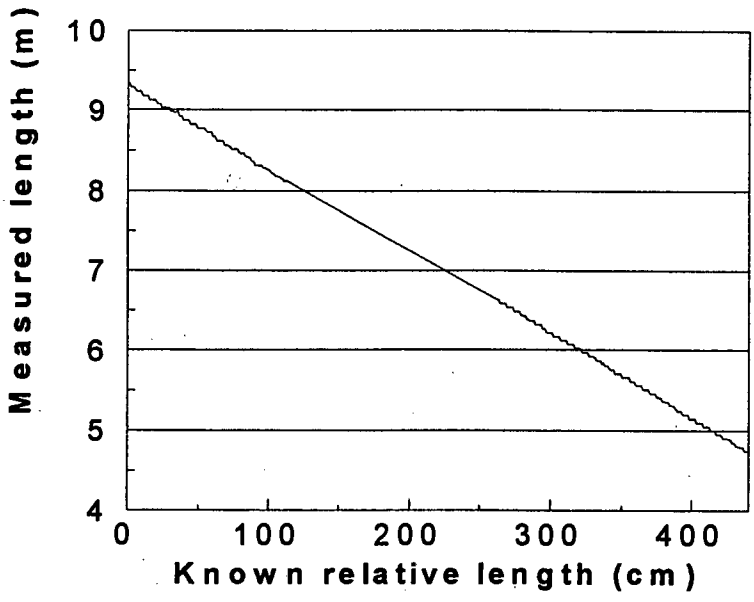

Figure 6.3: Extended length measurements.

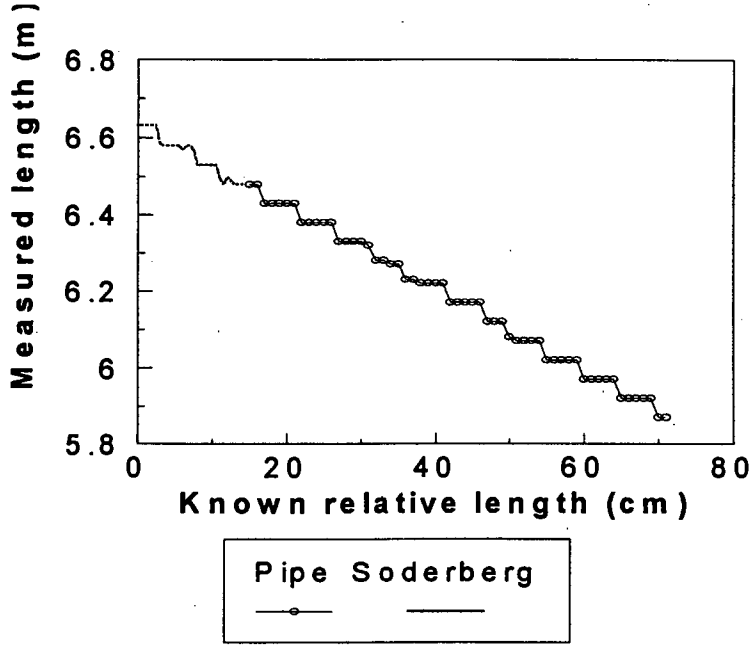

Figure 6.4: Length measurements though a section of Soderberg electrode.

Chapter 7

CONCLUSIONS

Based on the findings of this report, the following conclusions can be drawn:

- A microwave system in which a radar placed above the electrode is used to determine the electrode length has been identified as the most promising electrode-length-measurement technique.
- Both practical and theoretical evaluations have show that microwaves will be able to continue propagating in the cavity left in the electrode once the inserted waveguide has melted.
- A conventional frequency-modulated continuous wave radar provides the best overall performance in the furnace environment due to its ability to differentiate between targets, and the 'intelligence' with which it can be interfaced.
- The linearity of the microwave oscillator was found to be of critical importance in obtaining a high signal-to-noise ratio at the radar output.
- The fast Fourier transform provided both the resolution and robustness needed in the signal analysis of radar returns.
- The length of a hollow waveguide could be measured with an accuracy of 1.38cm over the range 4m to 9m using the system.
- The termination at the end of the pipe was found to be non-critical, with the system working well whether the pipe was terminated or not.
- The addition of a section of Soderberg electrode at the end of the steel tube did not affect the accuracy of the measurements. This shows firstly that the electromagnetic waves can propagate in a cavity in

the graphite electrode, and secondly that the reflection caused by the transition between the waveguide and the graphite cavity is small in comparison with the reflection caused at the end of the electrode.

The system now needs to be tested on a real furnace in order to evaluate the effects of the furnace environment more accurately.

Bibliography

[1] Ultrasonic wall-thickness measuring instrument. *Materials Evaluation*, 47:140, February 1989.

[2] A. B. Stewart. The Measurement of Electrical Variables in a Submerged-Arc Furnace. Technical report, National Institute for Technology, April 1981.

[3] A. Bas. *An Ultra High Resolution FMCW Radar.* MSc Thesis, University of Cape Town, 1992.

[4] A. E. Karbowiak. *Trunk Waveguide Communication.* Chapman and Hall LTD, 1965.

[5] A. W. D. Jongens. Personal communication. March 1994.

[6] C. W. Soderberg. Soderberg Self-Baking Continuous Electrodes. *Chemical and Metallurgical Engineering*, 26(25):1178–1182, June 1922.

[7] David K. Cheng. *Field and Wave Electromagnetics.* Addison-Wesley Publishing Company, 1989.

[8] John A. Dorr. Ultrasonic width measurement of continuously cast slabs. *Iron and Steel Engineer*, 69:33–36, October 1992.

[9] Merrill Skolnik. *Introduction to Radar Systems.* McGraw-Hill International editions, 1981.

[10] P. Horowitz and W. Hill. *The Art of Electronics.* Cambridge University Press, 1987.

[11] R. A. Waldron. *Theory of Guided Electromagnetic Waves.* Van Nostrand Reinhold Company, 1969.

[12] R. Innvaer, L. Olsen, A. Vatland. Operational Parameters for Soderberg Electrodes from Calculations, Measurements, and Plant experience. Technical report, Elkem R&D Center, Norway.

[13] S. A. Hovanessian. *Radar System Design and Analysis.* Artech House, 1984.

[14] Simon Haykin. *Adaptive Filter Theory.* Prentice Hall, 1991.

[15] Steven M. Kay and Stanley L. Marple. Spectrum Analysis-A modern Perspective. *Proceedings of the IEEE*, 69(11):1380–1419, November 1981.

[16] Watkins-Johnson Company. *RF and Microwave Components Designers' Handbook.* Watkins-Johnson, 1990.

Appendix A

Waveguide launcher design

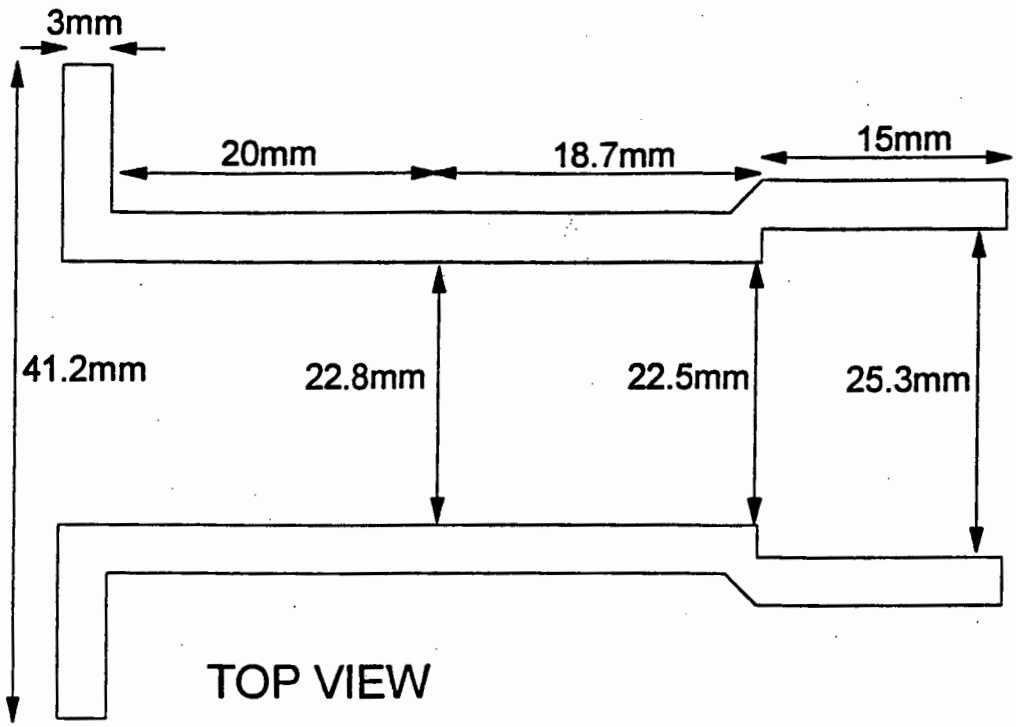

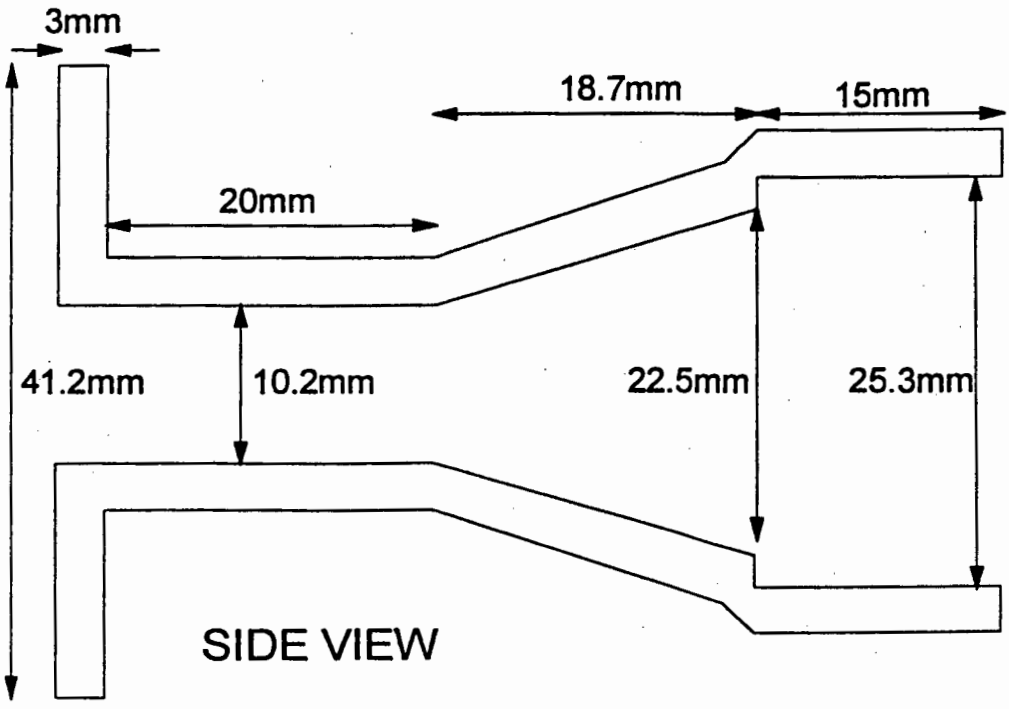

Appendix B

Low frequency circuit diagrams

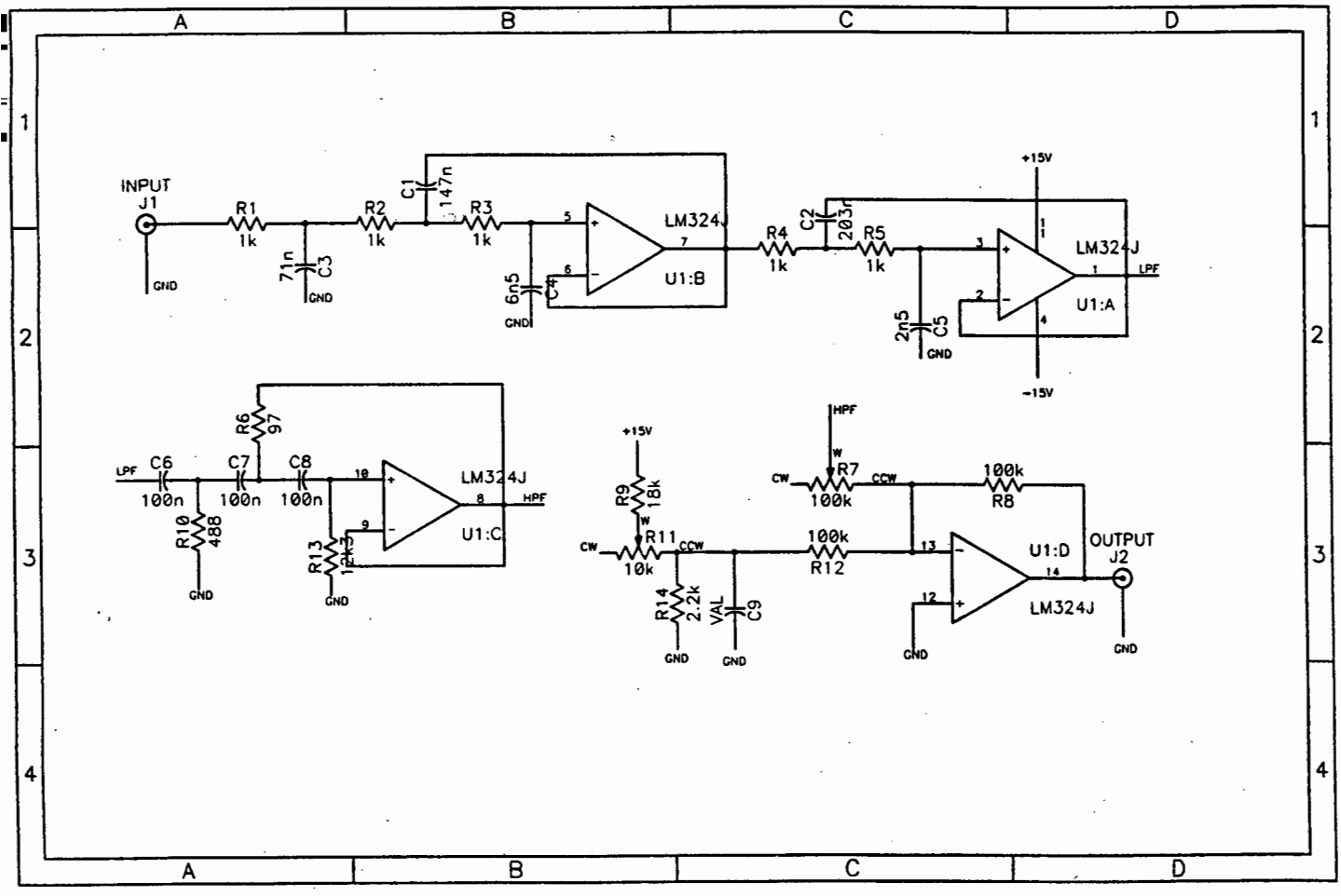

Appendix C

Description?

Circuit diagram of the interface card

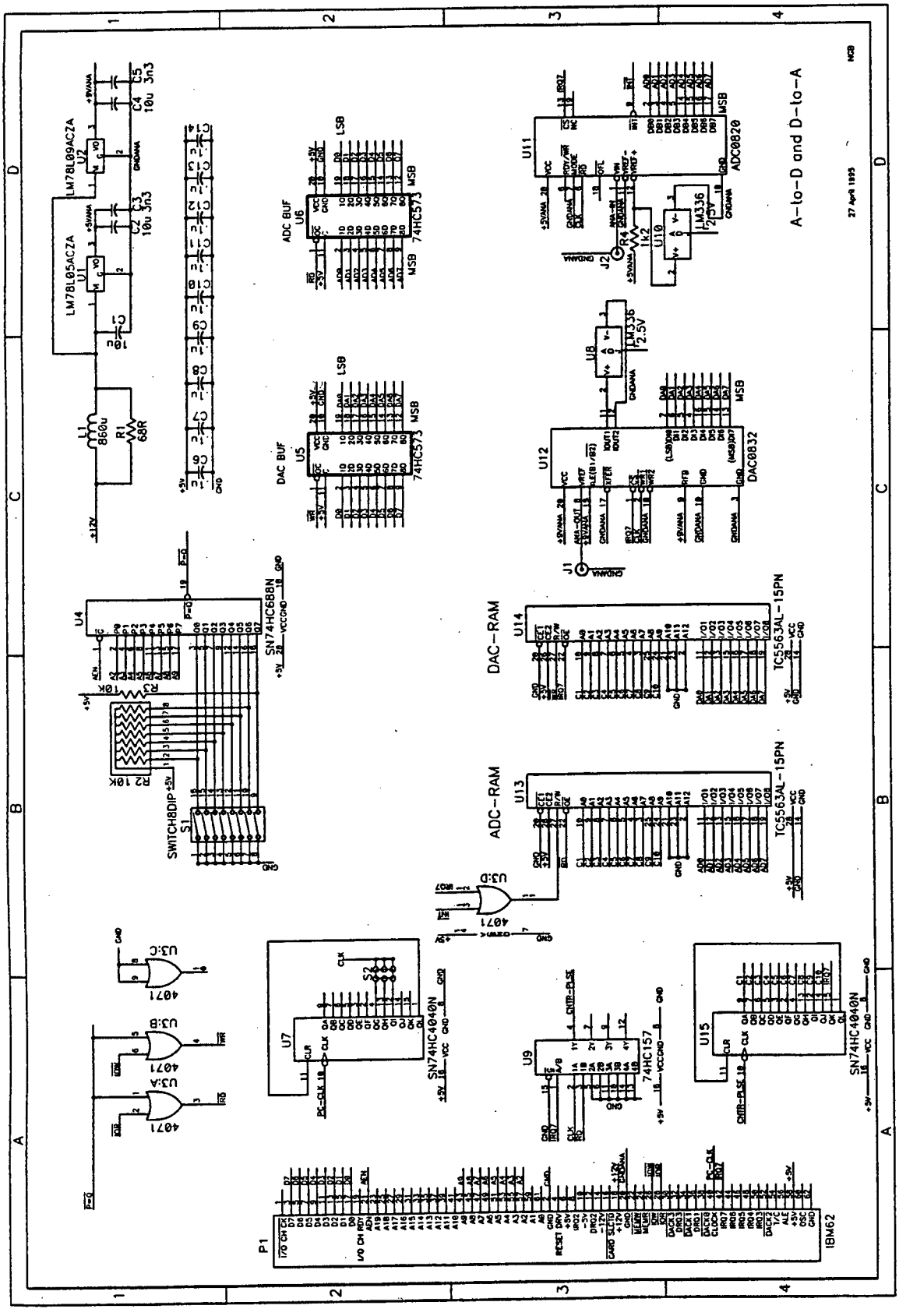

Appendix D

Signal processing techniques

Sampling frequency : $f_s := 10$

Number of time samples : $N := 64$ $n := 0..N-1$

Frequencies to be resolved : $f1 := 2$ $f2 := 2.2$

Creating the time funtion with added noise

$$wave1_n := \sin\left(\frac{2\cdot\pi\cdot f1\cdot n}{f_s}\right) + .1\cdot rnd(1) - .05 + \sin\left(\frac{2\cdot\pi\cdot f2\cdot n}{f_s}\right)$$

$$tot1 := \frac{\sum wave1}{N+1} \quad wave1_n := wave1_n - tot1$$

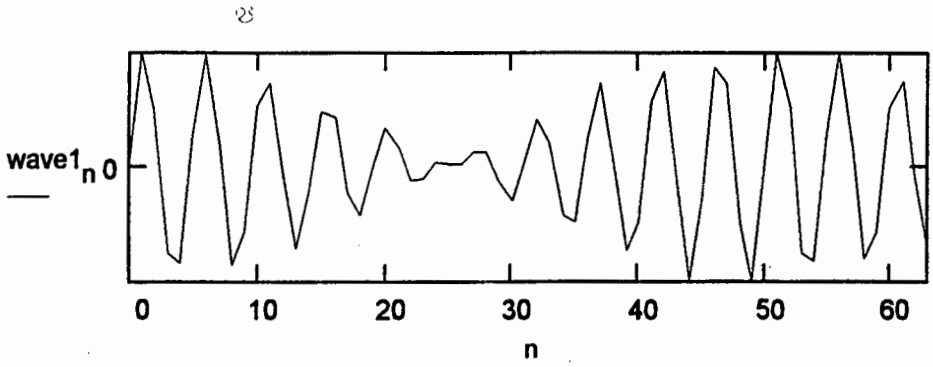

Apply the MUSIC method to the time domain function

Filter length $M := 5$ (0-4)

$x := 0..N-M-1$ $y := 0..M$ $sp_y := y$

$$A1_{h(y,x)} := wave1_{(M-y+x)}$$

$$A1_{h(y,x+N-M)} := wave1_{(x+y)}$$

$$A1 := \overline{A1_h{}^T} \qquad \phi 1 := A1_h \cdot A1 \qquad R1 := \frac{1}{2\cdot(N-M)}\cdot\phi 1$$

$ei1 := sort(eigenvals(R1))$ $v11 := eigenvec(R1, ei1_0)$

$V1_{n_{(y,0)}} := v11_y$ $V1_{nh} := \overline{V1_n}^T$

$S1(\omega) := \overrightarrow{e^{(-j \cdot \omega \cdot sp)}}$ $S1_h(\omega) := \overline{S1(\omega)}^T$

$DEN1(\omega) := \left| S1_h(\omega) \cdot V1_n \cdot V1_{nh} \cdot S1(\omega) \right|$

$$S1_{music}(f) := \frac{1}{DEN1\left(\frac{2 \cdot \pi \cdot f}{f_s}\right)}$$

Spectral plot of the time domain function using the MUSIC method

$spec := 0.01, .05 .. 5$

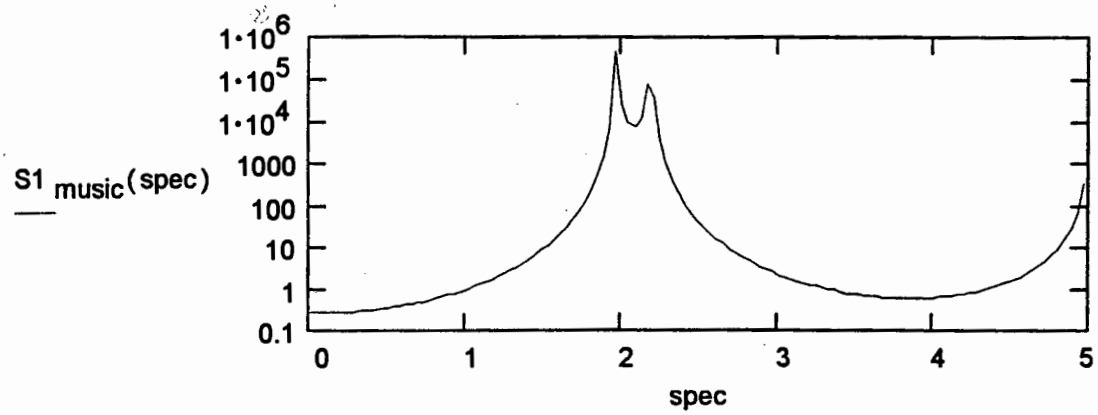

PRONY'S METHOD

Number of filter coefficients $P := 15$

Apply Prony's method to the time domain function

$s := 0 .. N - P - 1$ $p := 0 .. P - 1$

$pp := 0 .. P$ $po_{pp} := P - pp$

$b_{(s)} := -(wave1)_{(s+P)}$

$A_{(s,p)} := wave1_{(s+(P-1-p))}$

$a := \left(A^T \cdot A\right)^{-1} \cdot A^T \cdot b$

$c_0 := 1 \qquad c_{p+1} := a_p$

$zs(z) := \overrightarrow{z^{po}} \qquad poly(z) := zs(z) \cdot c$

Solving the spectral estimation function to obtain the frequency content :

$q1 := e^{\frac{2 \cdot \pi \cdot f1 \cdot j}{f_s}}$

$q2 := e^{\frac{2 \cdot \pi \cdot f2 \cdot j}{f_s}}$

$z1 := root(poly(q1), q1)$

$z2 := root(poly(q2), q2)$

$z1 = 0.3094 + 0.9509j$

$z2 = 0.1871 + 0.9817j$

$f1 := \frac{atan\left(\frac{Im(z1)}{Re(z1)}\right)}{2 \cdot \pi} \cdot f_s$

$f2 := \frac{atan\left(\frac{Im(z2)}{Re(z2)}\right)}{2 \cdot \pi} \cdot f_s$

Frequencies $f1 = 1.9993 \qquad f2 = 2.2002$

Magnitude of the spectral lines $|z1| = 0.9999 \qquad |z2| = 0.9994$

FAST FOURIER TRANSFORM

Apply the FFT to the time domain function :

$j := 0 .. \frac{N}{2}$

$fff := \overrightarrow{|fft(wave1)|} \qquad freq_j := j \cdot \frac{5}{\left(\frac{N}{2}\right)}$

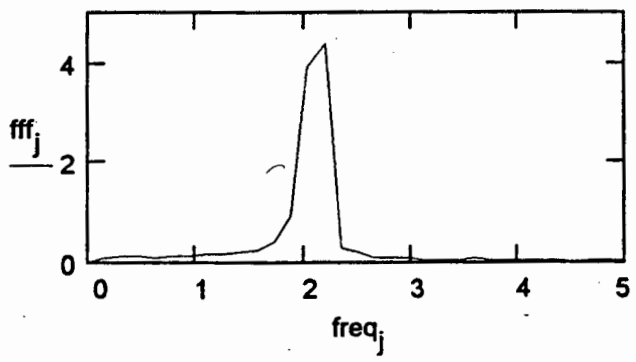

Appendix E

Program listing of RADAR.CPP

```
#include <io.h>
#include <stdio.h>
#include <stdlib.h>
#include <dos.h>
#include <conio.h>
#include <math.h>
#include <graphics.h>
#include <string.h>

#define INTR 0x0f      // ADCDA card interrupts on 7.
#define   CPPARGS ...
#define SWAP(a,b) tempr=(a);(a)=(b);(b)=tempr // Functi
  => on to swap a and b.

//-----------------------------------------------
//
//        GLOBAL VARIABLE DECLARATIONS
//-----------------------------------------------

int   midx,midy;
const no_elements = 4096;  // To store screen coords.
const no_aves = 20;        // No of time samples.
  => the FFT to average.   // The number of elements in
volatile int flag = 0;
  => t has occured (flag=1).  // Indicates that an interrup
float address_first = 0;   // Array address of maximum e
  => lement.
float ave_freq = 0;        // Average beat frequency.
int DAC_Data[1023];        // Data used to linearise the
  => oscillator.
int ADC_Data[1023];        // Data read in from the ADC,
  => FMCW radar info.
float ave_array[no_aves]; // Temporary storage to perfo
  => rm averaging.
float transformed[(no_elements*2)-1]; // Used to store
  => freq data after FFT.

void interrupt ( *oldhandler)(__CPPARGS);
unsigned int Original_INT_mask;

//-----------------------------------------------

void interrupt handler(__CPPARGS)

// This procedure is called each time an interrupt
// occurs.  The variable flag is triggered to
// indicate that an interrupt has been received.

{
  disable(); // Disable all interrupts.
  outportb(0x20, 0x67);
  flag=1;    // Set interrupt flag to affirmative.
  delay(10);
  enable(); // Re-enable the interrupts.
}

//-----------------------------------------------

void init_int()

// Sets interrupt controller so ADC-DAC card can
// indicate to PC that the on-board RAMS are full.
{
  oldhandler = getvect(INTR); // Save the old interrupt
  => vector.
  setvect(INTR, handler); // Install the new interrupt
  => vector.
  Original_INT_mask = inportb(0x21); // Set up 8259 PIC
  =>  chip for interrupt 7.
  outportb(0x21, Original_INT_mask & 0x7f );

    while (flag == 0) // Waiting for an initial interu
  => pt for synchronisation.
      {
      inportb(0x300); // Read trash data and increment t
  => he interface counter.
      }
}

//-----------------------------------------------

void close_int()
{
// Resets origional values to the interrupt
// controller before exitting the program.

  outportb(0x21, Original_INT_mask & 0xff);  // Disable
  =>  the interrupts
  setvect(INTR, oldhandler); // Restore the origional i
  => nterrupts as stored.
}

//-----------------------------------------------

void four1(float data[], unsigned long nn, int isign)

// Does a fast fourier transform on the sampled time
// domain data. This procedure comes from the C
// Recipes collection of algorithms.

{
    unsigned long n,mmax,m,j,istep,i;
    double wtemp,wr,wpr,wpi,wi,theta;
    float tempr,tempi;

    n=nn << 1;
    j=1;
    for (i=1;i<n;i+=2) {
        if (j > i) {
            SWAP(data[j],data[i]);
            SWAP(data[j+1],data[i+1]);
        }
        m=n >> 1;
        while (m >= 2 && j > m) {
            j -= m;
            m >>= 1;
        }
        j += m;
    }
    mmax=2;
    while (n > mmax) {
        istep=mmax << 1;
        theta=isign*(6.28318530717959/mmax);
        wtemp=sin(0.5*theta);
        wpr = -2.0*wtemp*wtemp;
        wpi=sin(theta);
        wr=1.0;
        wi=0.0;
        for (m=1;m<mmax;m+=2) {
            for (i=m;i<=n;i+=istep) {
                j=i+mmax;
                tempr=wr*data[j]-wi*dat
  => a[j+1];
                tempi=wr*data[j+1]+wi*d
  => ata[j];

                data[j]=data[i]-tempr;
                data[j+1]=data[i+1]-tem

  => p;

                data[i] += tempr;
                data[i+1] += tempi;
            }
            wr=(wtemp=wr)*wpr-wi*wpi+wr;
            wi=wi*wpr+wtemp*wpi+wi;
        }
        mmax=istep;
    }
}

//-----------------------------------------------

void DAC_File_Load()

// Loads data for linearising the RF oscillator from
// a file called IN_DAC.DAT.  The data is in an ASCII
// file of floats in a list.

{
FILE *fp;
float temp;

fp=fopen("IN_DAC.DAT","r");// points to open file.
    for(int i=0; i< 1024; i++)
      {
        fscanf(fp,"%f",&temp); // Load a single
  =>  time sample.
        DAC_Data[i]=temp; // Store the data val
  => ue in an array.
      }
    fclose(fp);
}

//-----------------------------------------------

void ADC_File_Save()

// Saves the FFT data in a file before exitting.

{
FILE *fp;

    fp=fopen("OUT_ADC.DAT","w");    // fp is a poin
  => ter to the open file.
```

```
        for(int i=0; i< 2*no_elements; i++)
        {
                fprintf(fp,"%f\n",transformed[i]);
        }
        fclose(fp);   // Store frequency data.
}


//-----------------------------------------------


void load_DAC()

// Loads the linearising function into the DAC RAM.
// The VCO is then linearised with this function.

{

flag = 0;
for (int i = 0; i<1024; i++)
   {
     inportb(0X300); // Read from the interface is done
  => to increment counter.
     outportb(0x300,DAC_Data[i]);  // Load function int
  => o RAMS on interface.
     printf("Data out = %d\n",DAC_Data[i]);
   }
}



//-----------------------------------------------


void Read_RAM()

// Reads sampled time domain values from ADC RAM.

{

flag = 0;  // Reset interrupt indicator to negative.

for (int i = 0; i <1024; i++)
   {
     ADC_Data[i] = inportb(0x300);
   } // Read a value from the ADC RAM.
}



//-----------------------------------------------


void Calc_Freq()

// Calculates the dominant frequency contained in
// the fourier transformed data.  Displays length.

{

int temp=0;
float big=0,total=0,address=0,tot=0;
char range[15], *meter = " meters.";


for (int i =2048; i<2*no_elements; i++) // The last 204
  => 8 elements are
   {                                    // zero padded
  => to provide
    transformed[i]=0;                   // interpolatio
  => n of data once
   }                                    // FFT has been
  =>  done (ZERO PADDING).

for (i = 0; i <1024; i++)
   {
     transformed[temp] = ADC_Data[i];  // Fill in zero
  =>  imaginary values
     temp++;                           // for the time
  =>  domain function
     transformed[temp]=0;              // as required
  => by the FFT procedure.
     temp++;
   }

four1(transformed-1,no_elements,1); // Perform the Four
  => ier transform.

temp=0;
address_first=0;

for ( i = 0; i <(no_elements/2); i++)  // Convert from
  => Re, Im to ABS co-ords.
   {
     transformed[i] = sqrt(pow(transformed[temp],2)+po
  => w(transformed[temp+1],2));
     if ((transformed[i] > big)&(i>50)) // Ignore firs
  => t 50 due to large DC
      {                                 // component i
  => n FFT.
        big=transformed[i];  // Choose the largest ele
  => ment from the spectrum.
        address_first=i;  // Store the address of the
  => largest element.
      }
     temp++;
     temp++;
   }

address += transformed[address_first-1]*(address_first-
  => 1);
address += transformed[address_first]*address_first;
address += transformed[address_first+1]*(address_first+
  => 1);
total = transformed[address_first-1]+transformed[addres
  => s_first]+transformed[address_first+1];
address=address/total;
// A weighted ave of largest 3 elements.

ave_freq=31.33*address/(0.5*no_elements); // Convert th
  => e FFT bin no to a freq.
tot = ave_freq;
ave_array[no_aves-1]=tot;

for (i = 0; i < (no_aves-1); i++) // Average no_aves ti
  => mes to obtain
   {                                // more accurate beat
  =>  freq.
    ave_array[i]=ave_array[i+1];
    tot=tot+ave_array[i];
   }
   tot=tot/no_aves;
   gcvt(tot*3.3338,3,range); // Convert from freq to ra
  => nge, and characterise.
   strcat(range,meter);      // Add the word "meters" t
  => o the measurement.
   cleardevice();
   outtextxy(midx,midy,range);  // Display the range in
  =>  the mid of screen.
   delay(100);
}


//-----------------------------------------------


 void main()
{ clrscr();

  init_int();  // enable and initiate interrupt 7.
  DAC_File_Load(); // Load the linearisation data.
  load_DAC();  // Send the modulation to the DAC RAM on
  =>  interface card.

  clrscr();

// CHANGING TO GRAPHICS MODE

int gdriver = DETECT, gmode, errorcode;  // Request aut
  => o detection
int size = 6;
initgraph(&gdriver, &gmode, "");  // Initialise graphic
  => s.
errorcode = graphresult();  // Read result of initialis
  => ation.
if (errorcode != grOk)  // An error occurred, so displa
  => ythe type of error.
{
   printf("Graphics error: %s\n", grapherrormsg(errorco
  => de));
   printf("Press any key to halt:");
   getch();
   exit(1); // Terminate with an error code.
}

midx = getmaxx() / 2; // Get middle screen co-ords.
midy = getmaxy() / 2;

settextjustify(CENTER_TEXT, CENTER_TEXT);  // Set text
  => attributes.
settextstyle(DEFAULT_FONT, HORIZ_DIR, size);

  while (!kbhit())  // Run until any key is pressed.
    {
      if (flag == 1)  // If an interrupt has occured, t
  => hen the ADC RAM is
       {Read_RAM();    // full (Sampling has been comple
  => ted).  Read the
        Calc_Freq();   // contents of the RAM and calcul
  => ate the range.
       }
    }
  ADC_File_Save();  // Save the last FFT data (just for
  => later inspection).
  close_int();      // This is useful for checking inte
  => rface performance.
}
```